

Supplementary Materials for

**Rapid molecular evolution of pain insensitivity
in multiple African rodents**

Ole Eigenbrod*, Karlien Y. Debus*, Jane Reznick, Nigel C. Bennett, Oscar Sánchez-Carranza, Damir Omerbašić, Daniel W. Hart, Alison J. Barker, Wei Zhong, Heike Lutermann, Jestina V. Katandukila, Georgies Mgone, Thomas J. Park, Gary R. Lewin†

*These authors contributed equally to this work.

†Corresponding author. Email: glewin@mdc-berlin.de

Published 31 May 2019, *Science* **364**, 852 (2019)

DOI: 10.1126/science.aau0236

This PDF file includes:

Materials and Methods
Figs. S1 to S9
Tables S1 to S4
Caption for Movie S1
References

Other Supplementary Material for this manuscript includes the following:

(available at science.sciencemag.org/content/364/6443/852/suppl/DC1)

Movie S1 (.mp4)

Materials and Methods

Animals

All animal protocols were approved by the University of Illinois at Chicago Institutional Animal Care and Use Committee, the German federal authorities (State of Berlin), or the Animal Use and Care Committee of the University of Pretoria, Republic of South Africa. Naked mole-rats used in this study were kept either at the Max-Delbrück Center for Molecular Medicine or at the University of Illinois at Chicago. All *Bathyergidae* species and East African root rats were housed at the University of Pretoria. Algogens in this study produce a very short duration pain behavior, as reflected in foot lifting or licking, that usually lasts less than 60 s in duration and was mostly over within the first 2-3 minutes following the injection. To avoid undue stress animals were normally confronted with only one algogen per day and most animals in this study were never confronted with more than two algogens in total. No long term adverse effects of algogen injections were ever observed in any of the animals used in this study.

Molecular Biology

The tissues analysed in this study were rapidly removed from euthanized animals and snap frozen in liquid nitrogen. Euthanasia was carried by first anesthetizing mole-rats with the inhalation anaesthetic halothane followed by cervical dislocation before the removal of tissues. Total RNA was isolated from the collected DRGs and spinal cord samples with TRIzol (Life Technologies) and dissolved in 30 μ L RNase-free water. Paired-end, strand-specific (dUTP) libraries were prepared from RNA samples isolated from three biological replicates per species and sequenced on the Illumina HiSeq2500 platform. For cDNA cloning 1–3 μ g total RNA was used to clone channel cDNAs amplified with specific primers from reverse transcribed material. The desired cDNA cloned into an IRES-dsRed or EGFP containing expression vector using the

SLIC reaction(44). Mutations were introduced by PCR and multiple-fragment SLIC cloning. In some cases, we obtained synthesized cDNAs constructs (GeneArt Invitrogen).

RNA sequencing and bioinformatic pipeline

Sequencing of cDNA libraries was done at the Scientific Genomics Platform at the Berlin Institute of Medical Systems Biology at the Max Delbrück Center. Sequencing yielded around 30 Mio read pairs per sample. Quality clipping of the raw reads was performed with Trimmomatic 0.32(45). Adapters were clipped off using 1 seed mismatch, a palindromic score threshold of 30 and a simple clip threshold of 15. Minimum quality for trailing bases was set to 20. Leading 10 bases were clipped to avoid bias introduced by random hexamer priming. Read pairs with at least one read shorter than 30 bases after quality clipping were discarded. Sequencing yielded 156 to 229 Mio quality clipped read pairs per species (see table 1). During quality clipping, between 1.6% and 2.1% of the read pairs were discarded per sample. RNAseq reads from *Bathyergidae* and the East African root rat were used for *de novo* transcriptome assembly. RNAseq reads were pooled per species to create the *de novo* transcriptome assembly. Transcriptomes from mouse (accession GCF 000001635.25, downloaded on 27/12/2016), naked mole-rat (accession GCF 000247695.1, downloaded on 29/12/2016) and Damaraland mole-rat (accession GCF 000743615.1, downloaded on 29/12/2016) were not assembled, as annotated sequence data were available from the RefSeq database(46). The Trinity tool (version 20140717)(17) and the Bridger software (version 2014-12-01)(16) were used with default parameters to assemble raw transcriptomes. Both assemblies were combined using the Contig Assembly Program version 3, CAP3(47) and all merged and non-merged sequences were used for downstream analyses. Sequencing library contamination in the assemblies were detected using BLASTn against mouse, naked mole-rat and human ribosomal and mitochondrial DNA sequences obtained from RefSeq

as well as sequences from bacterial genomes often found in laboratory samples(48). All assembled transcripts with a BLAST hit with an E-value $< 1e-20$ against ribosomal RNA, bacterial or mitochondrial DNA that covers at least 10% of the transcript were discarded. Transcripts putatively originating from human or mouse were discarded if they showed an E-value $< 1e-20$ and sequence identity of $> 99\%$ and covered at least 70% of the transcript.

Orthologous transcripts were identified by applying a reciprocal best hit strategy using a mouse protein data set derived from RefSeq(46) (accession number GCF 000001635.25, downloaded on 27/12/2016). Only the longest isoform per protein was considered for annotation. If available, protein sequences with experimental evidence (RefSeq-ID NP) were preferred over predicted sequences (RefSeq-ID XP). Cleaned transcript sequences were aligned against the mouse RefSeq protein data sets using BLASTx. All hits with an E-value $< 1e-20$ in forward direction and a sequence similarity of $\geq 75\%$ were considered for further analyses. The same stringency level was used for the alignment of protein sequences against the transcript sequences using tBLASTn. Putatively chimeric transcripts were discarded if multiple co-linear hits were identified using tBLASTn or BLASTx. Additionally, transcripts were excluded from downstream analysis if there was more than one protein with a best hit to that transcript (“collapse factor” > 1 (49)). Reciprocal best hits were computed and a full-length protein annotation was assigned if the BLASTx hit covered at least 80% of the protein sequence. Protein-coding transcripts identified by the reciprocal best hit strategy were extracted from the assembly as a reference transcriptome and further tested for assembly or annotation errors. TransRate was applied on each reference transcriptome, and sequences with more than 40% of the bases covered with mapped reads ($s(Ccov) > 0.4$) were kept for further analysis(50).

Transcriptome completeness is a measure that reflects what fraction of transcripts was recovered in the assembly and annotation process in comparison to a reference transcriptome. The completeness score was calculated using BUSCO (Benchmarking Universal Single-Copy Orthologs, version 1.22)(51) with the vertebrate data set as background in transcriptome mode. The E-value cutoff was set to 1e-20.

Orthologous transcripts in African mole-rats and other rodents were identified based on identical gene name. *De novo* assembled and annotated full-length transcripts from *Bathyergidae* species and the East African root rat were used as well as RefSeq mRNA sequences of other rodents, in which the longest gene isoform or, if available, an isoform with experimental support was selected. The transcriptome of *Fukomys darlingi* was generated based on published RNAseq reads from brain samples using the same assembly pipeline presented in this study(28).

Multiple sequence alignments were performed for all sets of orthologous sequences using Multiple Alignment using Fast Fourier Transform MAFFT (version 7.299b) in accurate mode (mafft-linsi)(52). The longest consecutive intersecting region per orthologous transcript was used for downstream analyses to focus on comparable regions of the assembled transcripts for phylogenetic tree reconstruction and transcript quantification. Only the region in the alignment between the first and the last base that could be aligned in all investigated species was used further. Additionally, any alignment regions with gaps longer than 100 nucleotides were removed as they might represent assembly errors. GUIDANCE2 (version 2.02)(53) was used to identify intersected alignments with falsely assigned sequences, and alignments with an average column score < 0.5 were excluded from further analysis.

The 6,427 orthologous protein-coding transcripts present in all 10 rodent species were used to reconstruct a phylogenetic tree, while *Mus musculus* and *Tachyoryctes splendens* were set as

outgroup species. A phylogenetic tree was calculated with a maximum likelihood (ML) approach implemented in the RAxML tool (version 8.2.3)(54). The general time reversible model was used to account for variable base frequencies and symmetrical substitution rates. A gamma distribution was assumed to underlie the rate heterogeneity over the sites. One hundred rapid bootstrap searches were performed in addition to 20 ML searches and the best ML tree was reported. Divergence times of rodent species were estimated using the mcmctree software of the PAML package(55). Fossil calibration for the divergence of *Muroidea* and *Ctenohystrica* was set to 47.6 to 59.2 Myr. Approximate likelihood calculations were performed due to the size of the alignment. The general time reversible model was chosen as a nucleotide substitution model. The MCMC (Markov chain Monte Carlo) search was run for 53,000 generations, while the first 3,000 generations were discarded as a burn-in and every fifth generation was sampled. Divergence times were stable across multiple repetitions of the calculations. The resulting phylogenetic tree was visualized using FigTree (version 1.4.2)(56).

Annotated transcriptomes of six *Bathyergidae* species, East African root rat and mouse were used as reference sequences for read count-based transcript quantification. *Heliophobius emini* and samples were excluded from quantitative analyses. The *Heliophobius emini* samples were excluded because of insufficient biological replicates as many library preparations failed from this species. We used single-linkage clustering of pairwise sample correlation based on logarithmized TPM (transcripts per million) values to cluster data from each tissue and species. When the *Cryptomys hottentotus mahali* samples were included, the data from dorsal root ganglia and spinal cord did not cluster cleanly, but rather with more distantly related species. Such an inaccurate clustering suggested to us that some of the sensory tissues were contaminated with non-sensory tissue during collection making expression data from these tissues unreliable.

Comparing transcript abundances between different species is a challenging task, as the quantification can be biased by the number of reference transcripts, transcript length, base composition and sequencing depth(57). The reference transcriptomes were prepared to create references with the same number of transcripts, approximately equal transcript lengths and base compositions to minimize the possible biases in transcript quantification. In total, the expression levels of 6,878 transcripts were compared between the East African root rat, mouse, naked mole-rat and five *Bathyergidae* species. Quality clipped reads were mapped to the curated transcriptomes. Bowtie2 (version 2.0.5)(58)was used to map the reads to the references. The second read of each pair had to map upstream of the reverse complement of the first paired read. Only paired alignments with the second read mapping to the reverse complement strand of the first read were allowed (parameters: --fr --nofw --no-discordant). After the alignment step, reads with a mapping quality lower than 30 were discarded using samtools (version 1.3)(59). Reads per transcript were quantified using eXpress (version 1.5.1)(60). Only read pairs from alignments with the first read on the reverse complement sequence and the second read on the forward strand were counted (parameter: --rf-stranded). Log-transformed transcripts per million values were used for data visualization, a pseudocount was added to the TPM values prior to applying the logarithm to avoid negative expression values. Estimated raw counts were normalized for library size with the TMM (trimmed mean of M values) method implemented in the edgeR tool for differential expression analysis(61, 62).

Multi-dimensional data like high-throughput transcript expression levels can be embedded in a two-dimensional space by t-SNE (t-distributed stochastic neighbor embedding) for quality control or clustering purposes(63). A quantitative comparison of transcriptomes was performed using spinal cord and dorsal root ganglion samples from eight rodent species. Transcript read

counts ($\log_2(\text{TPM}+1)$) were visualized using t-SNE implemented in the Rtsne package for R (Krijthe, J. Rtsne: T-distributed stochastic neighbor embedding using Barnes-Hut implementation. R package version 0.10, URL <http://CRAN.R-project.org/package=Rtsne> (2015)). Default parameters were used to embed the samples in two-dimensional space.

A neighbor joining tree based on euclidean distances of sample expression values per tissue was generated with the “visTreeBootstrap” function of the “supraHex” R package with 1000 bootstraps. Counts were transformed to logCPM (counts per million) and fed into a phylogenetic generalized least squares model (pGLS, “ppls” function from the “caper” R package(64)). A pGLS model was built per tissue and insensitivity type for each gene with the neighbor joining tree representing the sample distances. The allogen insensitivity of each sample was represented by a binary classifier in the pGLS model. Statistical significance of the model fit was evaluated by performing an ANOVA (analysis of variance), p-values of the F-test were adjusted for multiple testing afterwards using the Benjamini and Hochberg method. Genes were considered as differentially expressed if they showed an absolute mean log fold change larger than 1 and an adjusted p-value less than 0.05.

Multiple alignments of amino acid sequences of orthologous transcripts of 17 species were aligned and intersected to infer differences in selection pressure during evolutionary history (see Extended Data Table 4). Protein sequences were derived from the intersected transcripts using TransDecoder (version 2.0.1)(65) while only protein sequences in forward direction of the transcripts were considered. The longest predicted open reading frame per transcript was chosen as the representative protein-coding amino acid sequence. Peptide sequences were aligned using MAFFT (version 7.299b)(52), and codon alignments were generated with PAL2NAL (version 14)(66). Intersected coding sequences were then further processed with GUIDANCE2 (version

2.02)(53). Alignment columns with a score < 0.93 and whole alignments with an average column score < 0.9 were removed from the data set to focus on high quality annotated sequences and alignments.

We used CodeML from the PAML package (version 4.8)(55) to infer differences in selection pressures acting on specific branches of the phylogeny. Differences in selection pressure were inferred using a model that was designed to identify specific residues under divergent selection. Clade model C(67) tests for divergent selection by comparing the ratio of non-synonymous (dN) to synonymous substitutions (dS) in foreground versus background branches of the phylogenetic tree. Clade model C assumes three classes of sites within the codon alignment, while the model M2a_rel(68) serves as null model. Log-likelihood values of the two models were compared using a likelihood-ratio-test with one degree of freedom. Genes with a median distance between significant Bayes Empirical Bayes sites (BEB) (probability > 0.9) of 15 or lower were filtered out to correct for alignment errors. If only two BEB sites were detected, the filtering distance threshold was reduced to five. The false discovery rate was controlled for using the Benjamini and Hochberg method, and only genes with an adjusted p value < 0.05 and at least one significant BEB site were assumed to be under divergent selection.

Due to assembly errors like family collapse, where gene sequences from highly conserved gene families cannot be distinguished from each other on the basis of short reads, we were not able to assemble reliable transcripts for the SCN9A gene in most species. A guided assembly approach was used to retrieve the SCN9A sequences of *Bathyergidae* species and *Tachyoryctes splendens*. The SCN9A sequence of *Heterocephalus glaber* from RefSeq (XM_013076951.1) was used as a reference and DRG sample reads from *Tachyoryctes splendens*, *Heliophobius emini*, *Georchus capensis*, *Cryptomys hottentotus hottentotus*, *Cryptomys hottentotus mahali*, *Cryptomys*

hottentotus natalensis and *Cryptomys hottentotus pretoriae*, respectively, were mapped against it. Sensitive mapping setting for bowtie2 (version 2.0.5)(58) were chosen to account for sequence differences between the species (parameters --fr --nofw --nodiscordant --no-mixed --very-sensitive --score-min L,0,-1). Consensus sequences were created with samtools (version 1.3, mpileup and bcftools commands)(Li et al., 2009). Final coding sequences were derived with TransDecoder (version 2.0.1)(65) and then aligned with MAFFT (version 7.299b)(52). Jalview (version 2.9.0b2)(69) was used to visualize protein alignments.

Data from single-cell RNASeq sequencing experiments of DRG neurons was downloaded from <http://linnarssonlab.org/drg/>(19). A transcript was considered as expressed if the expression was >1 TPM in a cell. Cells were assigned to cell types according to Level 1 annotation of the scRNASeq study.

Cell culture and calcium imaging

HEK293 cells (used for electrophysiology) as well as AD293 cells (Agilent, used for calcium imaging) were cultured in DMEM/glutamax medium (Gibco) supplemented with 10% fetal calf serum and 1% penicillin and streptomycin. For single cell calcium imaging and electrophysiology, the cells were plated on PLL coated round glass coverslips (Roth) (10mm) and transfected after 24h with FUGENE (Promega). Imaging was performed typically one day after transfection, electrophysiology 48h after. Only EGFP and/or dsRed expressing cells were selected for electrophysiological recordings.

The calcium dye (CAL520® AM, AAT Bioquest, Inc.), a single wavelength calcium indicator, was dissolved in DMSO and 0.02% pluronic acid and loaded onto the cells one hour before the experiment. The coverslip was transferred to a custom made chamber, and perfused with extracellular buffer at room temperature for 10 – 20 minutes. Calcium imaging was carried out

with an Olympus BX51WI microscope equipped with the MetaFluor imaging system, including DG4 wavelength switcher (Sutter Instruments) and a CoolSNAP ES camera (Visitron). The settings were as follows: 20x water immersion objective, 14 bit resolution, sampling rate 3 seconds. The cells were excited with a 520 nm wavelength to see the red fluorescence from dsRed and a 480 nm for the Ca²⁺ indicator CAL520® AM. AITC was applied after 30 seconds of imaging for a period of 90 seconds. To normalize the signals, 1µM ionomycin was applied at the end.

High throughput Calcium imaging (FLIPR tetra)

Two days before measuring cells were plated in a black 384 well microplates with transparent bottom (Corning, 3683). 24h later they were in plate transfected using FuGENE (Promega). Per transfection mixture 64 wells were transfected, subjected to 8 different concentrations of AITC. Per TRPA1 species, at least 5 transfection mixtures were made in order to have minimum 40 wells measured per concentration. The transfection efficiency was tested one day later on a TECAN plate reader exciting with 556 nm and collecting the 586 nm wavelength. The values were used to calculate transfection outliers using the quartal method, which were excluded from further analysis. Fluo-4 (Thermofischer) was added one hour before the measurement and washed off with extracellular buffer (in mM: 140 NaCl, 4 glucose, 10 HEPES, 4 KCl, 2 CaCl₂, 1 mgCl₂, NaOH 5N until pH 7.4) right before placing the 384 well plates in the FLIPR device. Sampling rate was 1 second and AITC was added after 5 seconds. 180 seconds later ionomycin was added (final concentration 1µM).

qPCR

Total RNA was collected from tissues using ReliaPrep™ RNA Tissue Miniprep system (Promega), according to manufacturer's instructions. For reverse transcription with the

Superscript III reverse polymerase (Invitrogen) 0.5 µg of total RNA was taken and cDNA was analysed using the Universal Probe library (Roche) in a CFX384 Real Time PCR detection system. Primers to quantify Highveld and Natal mole-rat *NALCN* were F: 5'-TTCCAACAAATGTGGGGGTCA-3' R: 5'-TGCATCTTCGTGAAACATCTG-3' designed using the transcript sequences found doing RNAseq. The standard curve method with known doses of a plasmid containing the cDNA amplicon from the primer pair, was used to quantitate mRNA transcripts by extrapolating a value by comparing unknowns to the standard curve of known transcript amounts.

Electrophysiology

Whole cell patch clamp recordings were conducted on dsRed and/or EGFP-positive HEK293 cells 48 hours post transfection at room temperature. Patch pipettes were pulled from borosilicate glass capillaries and had a tip resistance of 3-6 MΩ. Pipette solution contained (in mM): 150 CsCl, 10 NaCl, 10 EGTA, 2 Mg₂ATP and 10 HEPES (pH 7.4, Osm ~320mOsm/L). Bath solution contained (in mM): 150 NaCl, 3.5 KCl, 2 MgCl₂, 1.2 CaCl₂, 10 HEPES, and 20 glucose (pH 7.4, Osm ~350mOsm/L). Recordings were made using EPC-9 amplifier (HEKA) and Patchmaster software (HEKA). A standard voltage-step protocol was used whereby cells were held at 0mV for 50 ms before stepping to the test potential -60mV – +60 mV (in 20mV increments) for 300ms, returning to the holding potential (0mV for 50 ms) between sweeps.

Performing current clamp, current pulses from -60pA to +20pA (20pA increments) were injected in the cell. The steady-state voltage responses were plotted against the amplitude of the current injection. The slope of the linear fit of this relationship was determined to calculate the input resistance.

Additional statistical analyses were performed using the GraphPad Prism software. Unless otherwise stated, a two-tailed unpaired t-test or Mann-Whitney test was employed, where * $p < 0.05$; ** $p < 0.01$; *** $p < 0.001$. All data are shown as mean ± SEM.

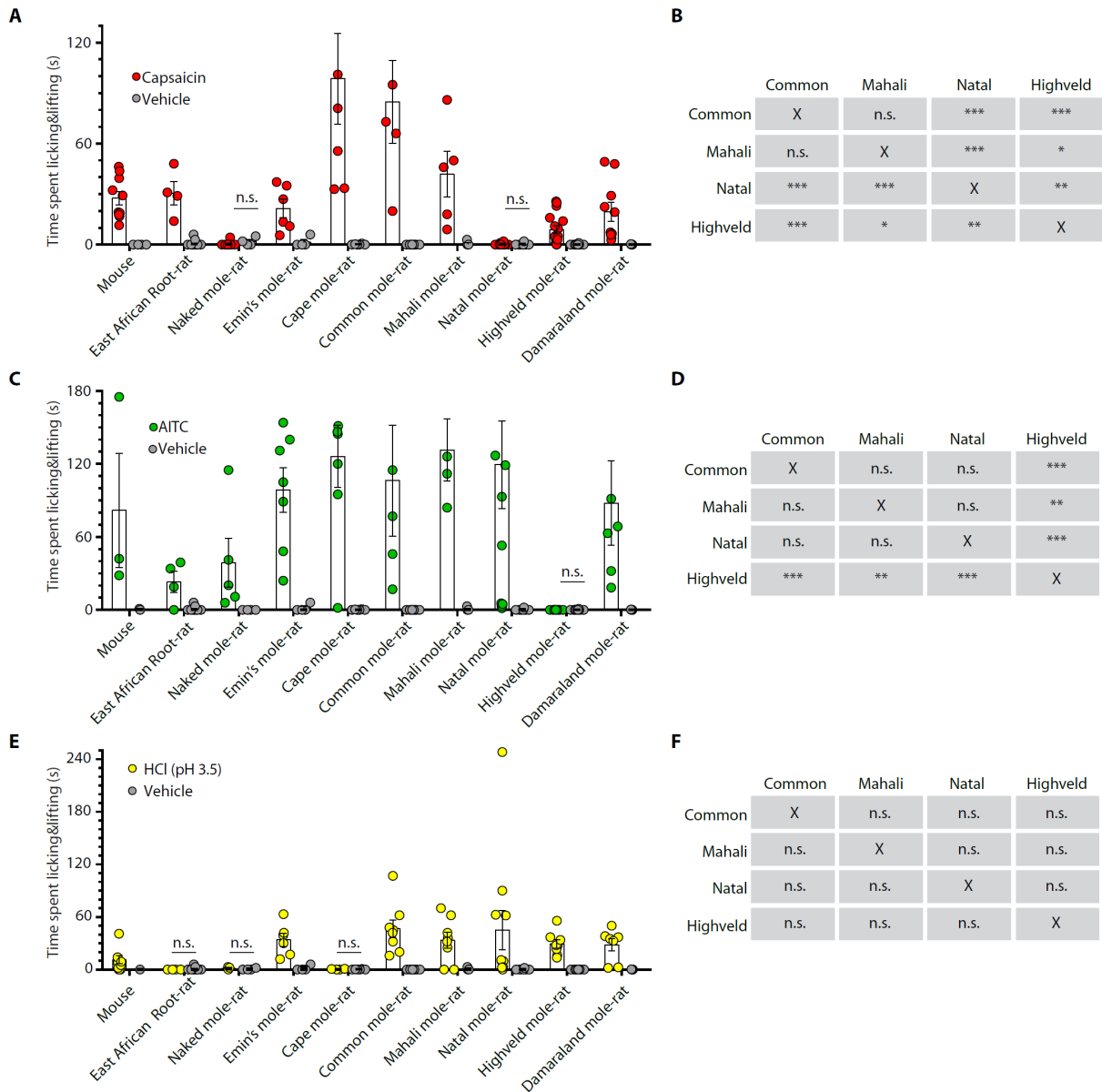


Fig. S1

Vehicle data and interspecies comparisons A) Summed response times for all species of rodents after capsaicin injection into the paw versus a vehicle injection (error bars indicate SEM; ns: $P > 0.05$; *Mann-Whitney U* test). B) Statistical comparisons within the genus. Note that Highveld mole-rats have a significantly blunted pain response to capsaicin compared to other *Cryptomys* species with the exception of the capsaicin insensitive Natal mole-rat. C) Summed response time of rodents upon injection of AITC to the paw plotted versus vehicle controls. D) Statistical comparisons within the genus. Note that all *Cryptomys* species with the exception of Highveld mole-rat have similar magnitudes of pain response to AITC. E) Cumulative response time of rodents upon injection of acid into the paw versus a vehicle injection (ns: $P > 0.05$; *Mann-Whitney U* test). F) Statistical comparisons within the genus. Note that all *Cryptomys* species showed a robust behavioral response to acid and there was no statistically significant differences within the genus *Cryptomys* (error bars indicate SEM; for all tests: ns: $P > 0.05$; * $P \leq 0.05$, ** $P \leq 0.01$, *** $P \leq 0.001$; *Mann-Whitney U* test)

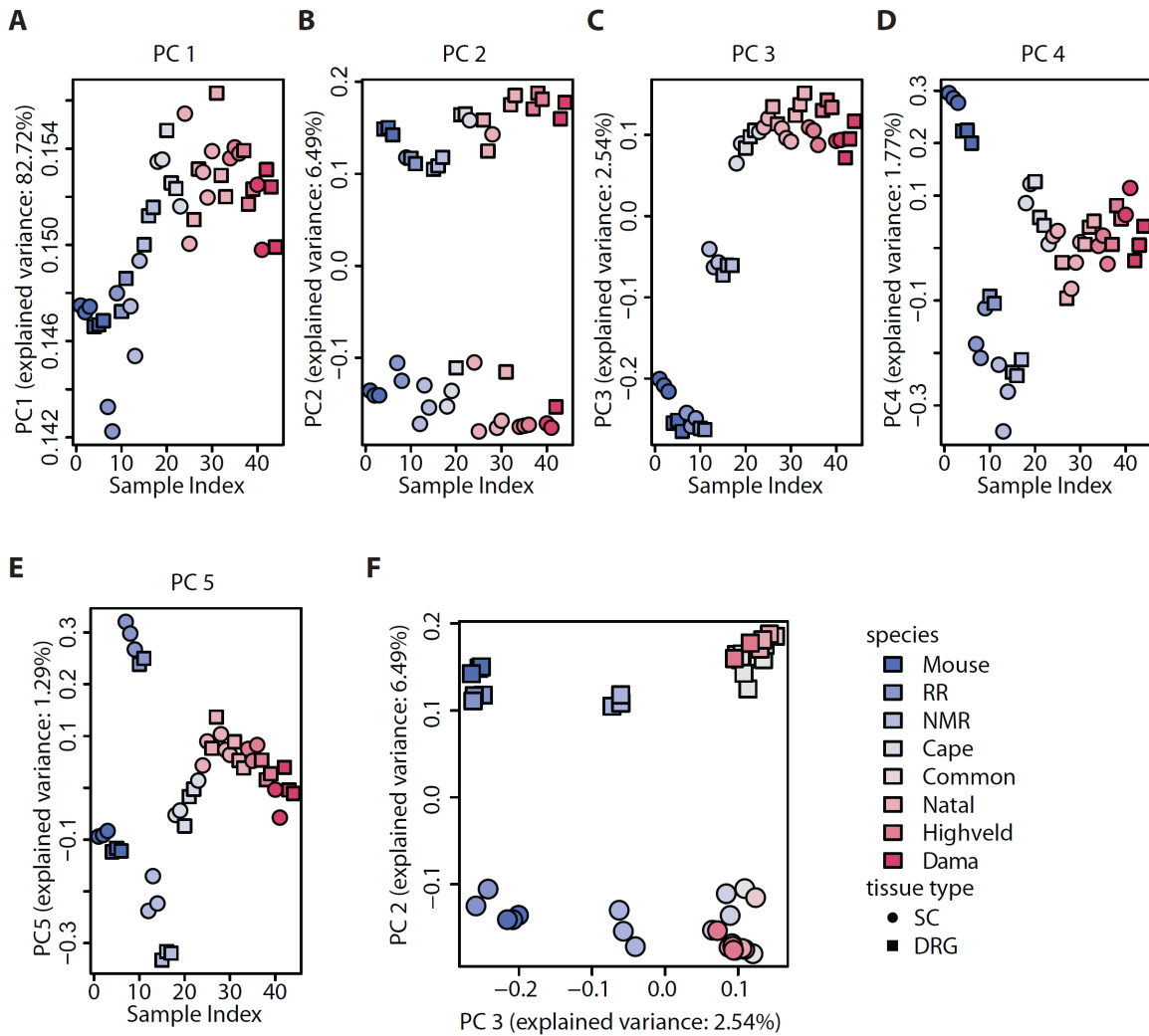


Fig S2

Principal component analysis (PCA) of transcript expression data. PCA values for the first five PCs. **A)** PC1 shows mostly biological variation across all samples with a slight phylogenetic component. **B)** PC2 clearly separates spinal cord from dorsal root ganglion samples. **C)** PC3 shows a phylogenetic signal, separating mice, root rats, naked mole-rats and the Bathyergidae species. **D)** PC4 seems to separate root rat and mouse spinal cord samples, while PC5 has the most extreme values for root rat and naked mole-rat. **E)** By plotting PC2 against PC3 a good separation of both tissues and species was achieved

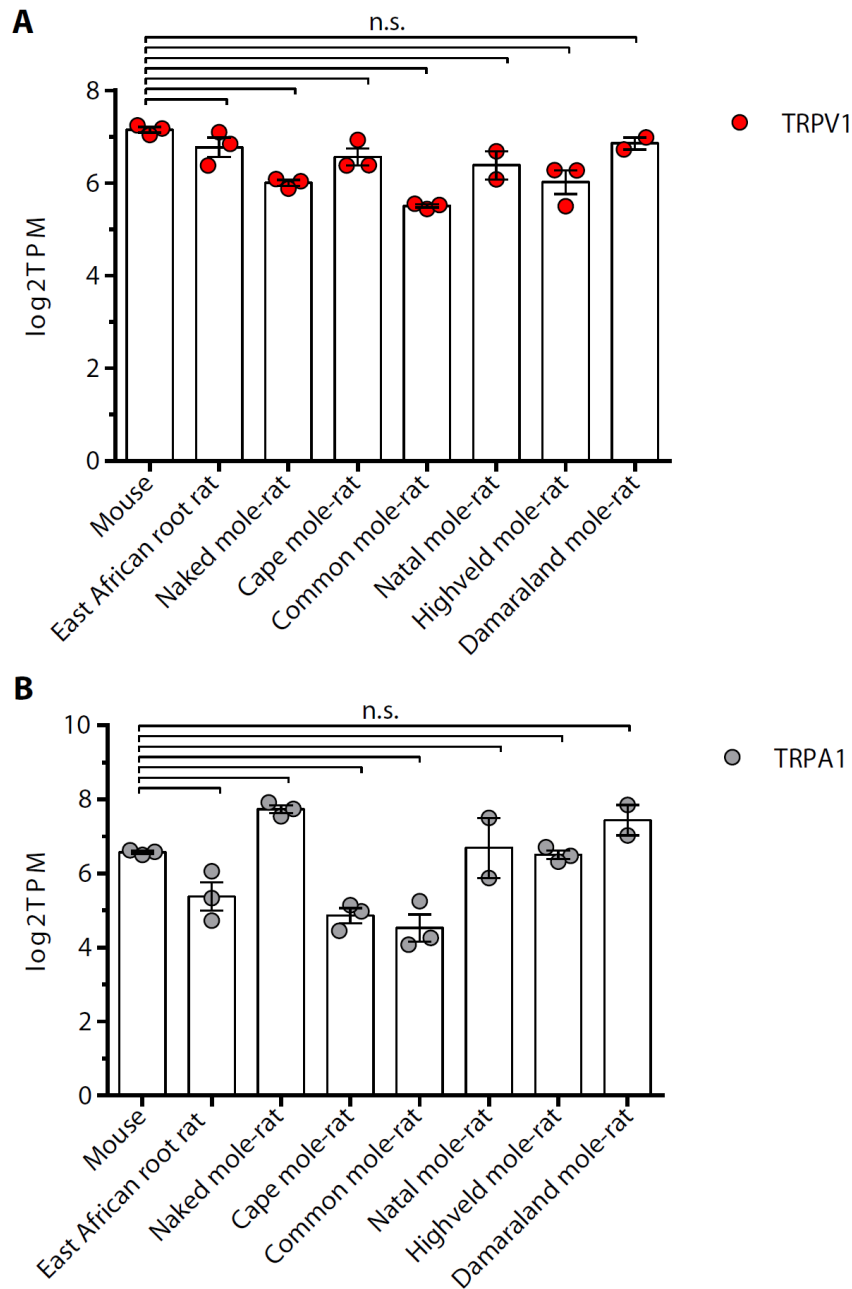


Fig. S3

TRPA1 and TRPV1 expression level in dorsal root ganglia. A) Log₂TPM values for TRPV1 in dorsal root ganglia from mouse, root rat and six *Bathyergidae* species show no significant difference between them. The same is shown for TRPA1 in B). There was no indication that TRPA1 or TRPV1 was differentially expressed in the DRG based on the pGLS model (see Figure 2), this was also the case when using a simple *Mann-Whitney U* test on the raw TPM values. Error bars indicate SEM;

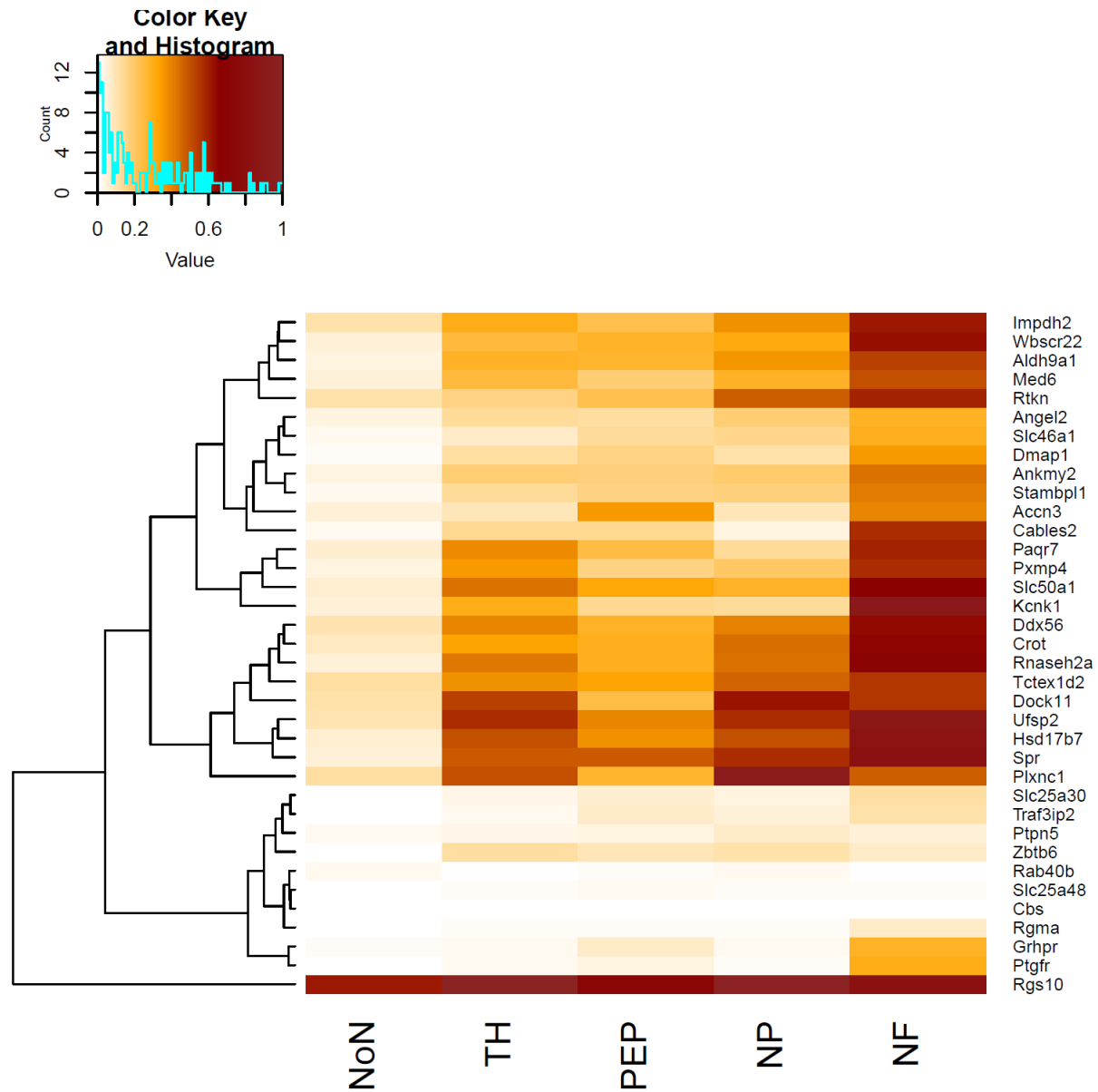


Fig. S4.

Cell-specific expression of differentially expressed genes in acid-insensitive species. Heatmap of the fraction of dorsal root ganglia cells that express transcripts identified as differentially expressed in the DRG of acid-insensitive species grouped by neuron type. Single-cell gene expression data was downloaded from (Usoskin et al., 2015).

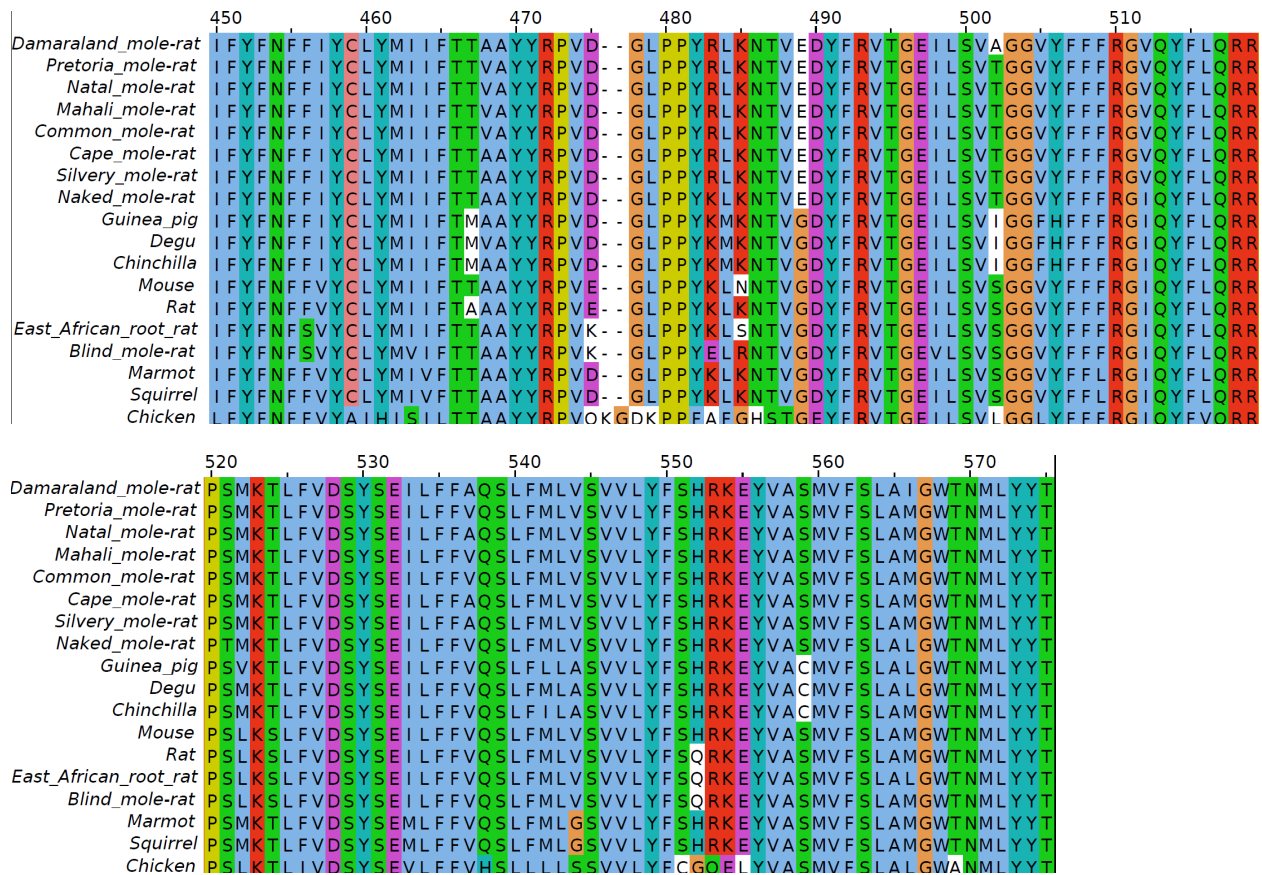


Fig. S5.

TRPV1 alignment S2-S4. Multiple protein sequence alignment of the TRPV1 ion channel in the putative capsaicin-binding region between the second and fourth transmembrane domain (S2-S4). Numbers on top of the alignment depict amino acid positions.

	581	622	772	975	1027	1086
<i>Freshwater planarian</i>	DKQGLTF	-GICPVI	AKKAVLV	KNANLKR	QVIYKKN	SDNI---
<i>Fruit fly</i>	NVLDMSA	KHPCVTL	RTTAILF	RNAQLKR	NPFTEDS	VDEG--
<i>Zebrafish</i>	NKNDASF	-KRCIVM	QSYLTTS	TNACLKR	WFFGGNE	HDGP---
<i>Japanese pufferfish</i>	NKSYTSF	-QRCPIV	QSLLLSF	RNASLKR	QLITGID	YDGPMLL
<i>Carolina anole</i>	NKSDASF	ANKCAIL	NSYFIKV	KFAVLKR	YCFGCD	EDTN---
<i>Collared flycatcher</i>	NKAVASF	ANKCPLL	DSYFTRV	KYAALKR	YCFGCED	EDSN---
<i>Red junglefowl</i>	NKAVASF	ANKCPLL	DSYFTRV	KYAALKR	YCFGCED	EDSN---
<i>American alligator</i>	NKAVASF	ANKCPLL	ESYFIRV	KYAALKR	YCFGCED	EDSN---
<i>Chinese softshell turtle</i>	NKASASF	SNKCPLL	DSYFIRV	KYAALKR	YCFGYED	EDSN---
<i>Ball python</i>	NKAEASF	INKCAIL	DSNFIKV	KFAAMKR	YCFGWDS	EDAA---
<i>Western diamondback rattlesnake</i>	NESEASF	INKCAIL	KSYFIKV	KFAAMKR	YCFGWDN	EDLN---
<i>Rhesus macaque</i>	NKQQASF	GNKCPIT	NSYLIKT	KHASLKR	FLFCTGE	EDNH---
<i>Human</i>	NKQQASF	GNKCPIT	NSYLIKT	KHASLKR	FLFCTGE	DDSH---
<i>Western gorilla</i>	NKQQASF	GNKCPIT	NSYLIKT	KHASLKR	FLFCTGE	DDSH---
<i>Common marmoset</i>	NKQQASF	GNKCPIT	DSYLIKT	KHASLKR	CLFCTGE	EDNH---
<i>Wild boar</i>	NKQRASF	SNRCPVM	NSYTIKV	KHALLKR	YIFCPQE	EDYQ---
<i>Horse</i>	NKQQASF	SNKCPIT	NSYSIKV	KHALLKR	HIFCPRE	EDNH---
<i>Sheep</i>	NKQQASF	TNRCPVI	NSYAINF	KHALLKR	YIFCPHE	EDYH---
<i>Cattle</i>	NKQQASF	TNRCPVI	NSFAINF	KHALLKR	YIFCPHE	EDYH---
<i>European rabbit</i>	NKQQASF	SNKCPIM	NSYPIKV	KHASLKR	YIFYINE	EDNH---
<i>Thirteen-lined ground squirrel</i>	NKQQASF	SNRCPTM	NSYAIQV	KHASLKR	YLFGSHE	EDNH---
<i>Alpine marmot</i>	NKQQASF	SNRCPTM	NSYAIQV	KHASLKR	YLFGSHE	EDNH---
<i>House mouse</i>	NKKQASF	SNRCPIM	NSFPIKI	KHASLKR	YFLNMQE	EDNH---
<i>Brown rat</i>	NKKQASF	SNRCPIM	NSFPLKI	KHASLKR	YFLSMQE	EDNH---
<i>Blind mole-rat</i>	NKQQASF	SNRCPIM	DSFPIKI	KHASLKR	YFLCTQE	EDNH---
<i>East-African mole-rat</i>	NKQQASF	SNRCPIM	DSFPIKI	KHASLKR	YFLCTQE	EDNH---
<i>Long-tailed chinchilla</i>	NKQKASF	SNKCPIM	NSYPIKV	KHASLKR	YFFGIQE	ADNH---
<i>Degu</i>	NKQQASF	SNKCPIM	NSYSIKV	KHASLKR	YFFGIQE	EDNH---
<i>Guinea pig</i>	NKQQASF	SNRCPIT	NSYPIKV	KHASLKR	YFFGVQE	EDNH---
<i>Naked mole-rat</i>	NKQRASF	SNRCPIM	NSYPIKV	KHASLKR	YFFGIQE	EDNH---
<i>Silvery mole-rat</i>	NKQRASF	SNRCPIM	KSYPIKV	KHASLKR	YFFGIQE	EDNH---
<i>Cape mole-rat</i>	NKQRASF	SNKCPVI	KSYPIKV	KHASLKR	YFFGIQE	EDNH---
<i>Common mole-rat</i>	NKQCASF	SNKFPVM	KSYGIKI	KHACLKR	YFFVIQE	EDNH---
<i>Mahali mole-rat</i>	NKQCASF	SNKFPVM	KSYGIKI	KHACLKR	YFFVIQE	EDNH---
<i>Natal mole-rat</i>	NKQCASF	SNKFPVM	KSYGINI	KHACLKR	YFFVIQE	EDNH---
<i>Pretoria mole-rat</i>	NKQCASF	SNKFPVM	KSYGIKI	KHACLKR	YFFVIQE	EDNH---
<i>Damaraland mole-rat</i>	NKQWASF	SNKCPVM	NSYPIKV	KHASLKR	YFFGIQE	EDNH---

Fig. S6. Cryptomys-specific variants in TRPA1. Multiple protein sequence alignment of the TRPA1 ion channel. Regions were selected based on *Cryptomys*-specific variants in the protein. Numbers on top of the alignment depict amino acid positions.

Danio_erio MCSAGAISALLFPLIHSLYSTASPSMLKRKQSSRVEAQPMTDFGPDDELTDSDADILWINK 60
Marmota_marmota -----MLKRKQSSRVEAQPVTDFGPDDELSDNADILWINK 35
Tachyoryctes_splendens -----MLKRKQSSRVEAQPVTDFGPDDELSDNADILWINK 35
Rattus_norvegicus -----MLKRKQSSRVEAQPVTDFGPDDELSDNADILWINK 35
Mus_musculus -----MLKRKQSSRVEAQPVTDFGPDDELSDNADILWINK 35
Nannospalax_galili -----MLKRKQSSRVEAQPVTDFGPDDELSDNADILWINK 35
Homo_sapiens -----MLKRKQSSRVEAQPVTDFGPDDELSDNADILWINK 35
Pan_troglodytes -----MLKRKQSSRVEAQPVTDFGPDDELSDNADILWINK 35
Cavia_porcellus -----MLKRKQSSRVEAQPVTDFGPDDELSDNADILWINK 35
Heterocephalus_glaber -----MLKRKQSSRVEAQPVTDFGPDDELSDNADILWINK 35
Georychus_capensis -----MLKRKQSSRVEAQPVTDFGPDDELSDNADILWINK 35
Heliophobius_emini -----MLKRKQSSRVEAQPVTDFGPDDELSDNADILWINK 35
Fukomys_damarensis -----MLKRKQSSRVEAQPVTDFGPDDELSDNADILWINK 35
Cryptomys_hottentotus_hottentotus -----MLKRKQSSRVEAQPVTDFGPDDELSDNADILWINK 35
Cryptomys_hottentotus_mahali -----MLKRKQSSRVEAQPVTDFGPDDELSDNADILWINK 35
Cryptomys_hottentotus_pretoriae -----MLKRKQSSRVEAQPVTDFGPDDELSDNADILWINK 35
Cryptomys_hottentotus_natalensis -----MLKRKQSSRVEAQPVTDFGPDDELSDNADILWINK 35
*****.*****.*****.*****.*****

Danio_erio PWVHSLLRACAIISVISVCMNTPKTFEHYPPQLQYVTFALDITLLMFLYTAEMIAKMHIRGI 120
Marmota_marmota PWVHSLLRICAISVISVCMNTPMTFEHYPPQLQYVTFDITLLMFLYTAEMIAKMHIRGI 95
Tachyoryctes_splendens PWVHSLLRICAISVISVCMNTPMTFEHYPPQLQYVTFDITLLMFLYTAEMIAKMHIRGI 95
Rattus_norvegicus PWVHSLLRICAISVISVCMNTPMTFEHYPPQLQYVTFDITLLMFLYTAEMIAKMHIRGI 95
Mus_musculus PWVHSLLRICAISVISVCMNTPMTFEHYPPQLQYVTFDITLLMFLYTAEMIAKMHIRGI 95
Nannospalax_galili PWVHSLLRICAISVISVCMNTPMTFEHYPPQLQYVTFDITLLMFLYTAEMIAKMHIRGI 95
Homo_sapiens PWVHSLLRICAISVISVCMNTPMTFEHYPPQLQYVTFDITLLMFLYTAEMIAKMHIRGI 95
Pan_troglodytes PWVHSLLRICAISVISVCMNTPMTFEHYPPQLQYVTFDITLLMFLYTAEMIAKMHIRGI 95
Cavia_porcellus PWVHSLLRICAISVISVCMNTPMTFEHYPPQLQYVTFDITLLMFLYTAEMIAKMHIRGI 95
Heterocephalus_glaber PWVHSLLRICAISVISVCMNTPMTFEHYPPQLQYVTFDITLLMFLYTAEMIAKMHIRGI 95
Georychus_capensis PWVHSLLRICAISVISVCMNTPMTFEHYPPQLQYVAFALDITLLMFLYTAEMIAKMHIRGI 95
Heliophobius_emini PWVHSLLRICAISVISVCMNTPMTFEHYPPQLQYVAFALDITLLMFLYTAEMIAKMHIRGI 95
Fukomys_damarensis PWVHSLLRICAISVISVCMNTPMTFEHYPPQLQYVAFALDITLLMFLYTAEMIAKMHIRGI 95
Cryptomys_hottentotus_hottentotus PWVHSLLRICAISVISVCMNTPMTFEHYPPQLQYVAFALDITLLMFLYTAEMIAKMHIRGI 95
Cryptomys_hottentotus_mahali PWVHSLLRICAISVISVCMNTPMTFEHYPPQLQYVAFALDITLLMFLYTAEMIAKMHIRGI 95
Cryptomys_hottentotus_pretoriae PWVHSLLRICAISVISVCMNTPMTFEHYPPQLQYVAFALDITLLMFLYTAEMIAKMHIRGI 95
Cryptomys_hottentotus_natalensis PWVHSLLRICAISVISVCMNTPMTFEHYPPQLQYVAFALDITLLMFLYTAEMIAKMHIRGI 95
*****.*****.*****.*****.*****

Danio_erio IKGENSYVKDRWCDFGFMVFLWVSLVQLQVFEIADIVDQMSPWGMLRIPRPLIMIRAFR 180
Marmota_marmota VKGDSSYVKDRWCDFGFMVFLWVSLVQLQVFEIADIVDQMSPWGMLRIPRPLIMIRAFR 155
Tachyoryctes_splendens VKGDSSYVKDRWCDFGFMVFLWVSLVQLQVFEIADIVDQMSPWGMLRIPRPLIMIRAFR 155
Rattus_norvegicus VKGDSSYVKDRWCDFGFMVFLWVSLVQLQVFEIADIVDQMSPWGMLRIPRPLIMIRAFR 155
Mus_musculus VKGDSSYVKDRWCDFGFMVFLWVSLVQLQVFEIADIVDQMSPWGMLRIPRPLIMIRAFR 155
Nannospalax_galili VKGDSSYVKDRWCDFGFMVFLWVSLVQLQVFEIADIVDQMSPWGMLRIPRPLIMIRAFR 155
Homo_sapiens VKGDSSYVKDRWCDFGFMVFLWVSLVQLQVFEIADIVDQMSPWGMLRIPRPLIMIRAFR 155
Pan_troglodytes VKGDSSYVKDRWCDFGFMVFLWVSLVQLQVFEIADIVDQMSPWGMLRIPRPLIMIRAFR 155
Cavia_porcellus VKGDSSYVKDRWCDFGFMVFLWVSLVQLQVFEIADIVDQMSPWGMLRIPRPLIMIRAFR 155
Heterocephalus_glaber VKGDSSYVKDRWCDFGFMVFLWVSLVQLQVFEIADIVDQMSPWGMLRIPRPLIMIRAFR 155
Georychus_capensis VKGDSSYVKDRWCDFGFMVFLWVSLVQLQVFEIADIVDQMSPWGMLRIPRPLIMIRAFR 155
Heliophobius_emini VKGDSSYVKDRWCDFGFMVFLWVSLVQLQVFEIADIVDQMSPWGMLRIPRPLIMIRAFR 155
Fukomys_damarensis VKGDSSYVKDRWCDFGFMVFLWVSLVQLQVFEIADIVDQMSPWGMLRIPRPLIMIRAFR 155
Cryptomys_hottentotus_hottentotus VKGDSSYVKDRWCDFGFMVFLWVSLVQLQVFEIADIVDQMSPWGMLRIPRPLIMIRAFR 155
Cryptomys_hottentotus_mahali VKGDSSYVKDRWCDFGFMVFLWVSLVQLQVFEIADIVDQMSPWGMLRIPRPLIMIRAFR 155
Cryptomys_hottentotus_pretoriae VKGDSSYVKDRWCDFGFMVFLWVSLVQLQVFEIADIVDQMSPWGMLRIPRPLIMIRAFR 155
Cryptomys_hottentotus_natalensis VKGDSSYVKDRWCDFGFMVFLWVSLVQLQVFEIADIVDQMSPWGMLRIPRPLIMIRAFR 155
:*.*****.*****.*****.*****.*****

Danio_erio IYRFELPRTRITNILKRSGEQIWSVSIFLFFLLYLGILVQMGFTFYHCVVNDTKPG 240
Marmota_marmota IYRFELPRTRITNILKRSGEQIWSVSIFLFFLLYLGILVQMGFTFYHCVVNDTKPG 215
Tachyoryctes_splendens IYRFELPRTRITNILKRSGEQIWSVSIFLFFLLYLGILVQMGFTFYHCVVNDTKPG 215
Rattus_norvegicus IYRFELPRTRITNILKRSGEQIWSVSIFLFFLLYLGILVQMGFTFYHCVVNDTKPG 215
Mus_musculus IYRFELPRTRITNILKRSGEQIWSVSIFLFFLLYLGILVQMGFTFYHCVVNDTKPG 215
Nannospalax_galili IYRFELPRTRITNILKRSGEQIWSVSIFLFFLLYLGILVQMGFTFYHCVVNDTKPG 215
Homo_sapiens IYRFELPRTRITNILKRSGEQIWSVSIFLFFLLYLGILVQMGFTFYHCVVNDTKPG 215
Pan_troglodytes IYRFELPRTRITNILKRSGEQIWSVSIFLFFLLYLGILVQMGFTFYHCVVNDTKPG 215
Cavia_porcellus IYRFELPRTRITNILKRSGEQIWSVSIFLFFLLYLGILVQMGFTFYHCVVNDTKPG 215
Heterocephalus_glaber IYRFELPRTRITNILKRSGEQIWSVSIFLFFLLYLGILVQMGFTFYHCVVNDTKPG 215
Georychus_capensis IYRFELPRTRITNILKRSGEQIWSVSIFLFFLLYLGILVQMGFTFYHCVVNDTKPG 215
Heliophobius_emini IYRFELPRTRITNILKRSGEQIWSVSIFLFFLLYLGILVQMGFTFYHCVVNDTKPG 215
Fukomys_damarensis IYRFELPRTRITNILKRSGEQIWSVSIFLFFLLYLGILVQMGFTFYHCVVNDTKPG 215
Cryptomys_hottentotus_hottentotus IYRFELPRTRITNILKRSGEQIWSVSIFLFFLLYLGILVQMGFTFYHCVVNDTKPG 215
Cryptomys_hottentotus_mahali IYRFELPRTRITNILKRSGEQIWSVSIFLFFLLYLGILVQMGFTFYHCVVNDTKPG 215

Homo_sapiens VDVIVAASNYKGENFRRQYDEFYLAEVAFTVLFDEALLKIWCLGFTGYISSSLHKFEL 455
Pan_troglodytes VDVIVAASNYKGENFRRQYDEFYLAEVAFTVLFDEALLKIWCLGFTGYISSSLHKFEL 455
Cavia_porcellus VDVIVAASNYKGENFRRQYDEFYLAEVAFTVLFDEALLKIWCLGFTGYISSSLHKFEL 455
Heterocephalus_glaber VDVIVAASNYKGENFRRQYDEFYLAEVAFTVLFDEALLKIWCLGFTGYISSSLHKFEL 455
Georchus_capensis VDVIVAASNYKGENFRRQYDEFYLAEVAFTVLFDEALLKIWCLGFTGYISSSLHKFEL 455
Heliophobius_emini VDVIVAASNYKGENFRRQYDEFYLAEVAFTVLFDEALLKIWCLGFTGYISSSLHKFEL 455
Fukomys_damarensis VDVIVAASNYKGENFRRQYDEFYLAEVAFTVLFDEALLKIWCLGFTGYISSSLHKFEL 455
Cryptomys_hottentotus_hottentotus VDVIVAASNYKGENFRRQYDEFYLAEVAFTVLFDEALLKIWCLGFTGYISSSLHKFEL 455
Cryptomys_hottentotus_mahali VDVIVAASNYKGENFRRQYDEFYLAEVAFTVLFDEALLKIWCLGFTGYISSSLHKFEL 455
Cryptomys_hottentotus_pretoriae VDVIVAASNYKGENFRRQYDEFYLAEVAFTVLFDEALLKIWCLGFTGYISSSLHKFEL 455
Cryptomys_hottentotus_natalensis VDVIVAASNYKGENFRRQYDEFYLAEVAFTVLFDEALLKIWCLGFTGYISSSLHKFEL 455
*****:~: *****

Danio_riero LLVVGTTLHVYPDLHSQFTYFQVLRVRLIKISPALEDFVYKIFGPGKKGSLVVFAS 538
Marmota_marmota LLVVGTTLHVYPDLHSQFTYFQVLRVRLIKISPALEDFVYKIFGPGKKGSLVVFAS 515
Tachyoryctes_splendens LLVVGTTLHVYPGLYHSQFTYFQVLRVRLIKISPALEDFVYKIFGPGKKGSLVVFAS 515
Rattus_norvegicus LLVIGTTLHVYPDLHSQFTYFQVLRVRLIKISPALEDFVYKIFGPGKKGSLVVFAS 515
Mus_musculus LLVIGTTLHVYPDLHSQFTYFQVLRVRLIKISPALEDFVYKIFGPGKKGSLVVFAS 515
Nannospalax_galili LLVIGTTLHVYPGLYHSQFTYFQVLRVRLIKISPALEDFVYKIFGPGKKGSLVVFAS 515
Homo_sapiens LLVIGTTLHVYPDLHSQFTYFQVLRVRLIKISPALEDFVYKIFGPGKKGSLVVFAS 515
Pan_troglodytes LLVIGTTLHVYPDLHSQFTYFQVLRVRLIKISPALEDFVYKIFGPGKKGSLVVFAS 515
Cavia_porcellus LLVVGTTLHVYPDLHSQFTYFQVLRVRLIKISPALEDFVYKIFGPGKKGSLVVFAS 515
Heterocephalus_glaber LLVIGTTLHVYPDLHSQFTYFQVLRVRLIKISPALEDFVYKIFGPGKKGSLVVFAS 515
Georchus_capensis LLVIGTTLHVYPDLHSQFTYFQVLRVRLIKISPALEDFVYKIFGPGKKGSLVVFAS 515
Heliophobius_emini LLVIGTTLHVYPDLHSQFTYFQVLRVRLIKISPALEDFVYKIFGPGKKGSLVVFAS 515
Fukomys_damarensis LLVIGTTLHVYPDLHSQFTYFQVLRVRLIKISPALEDFVYKIFGPGKKGSLVVFAS 515
Cryptomys_hottentotus_hottentotus LLVIGTTLHVYPDLHSQFTYFQVLRVRLIKISPALEDFVYKIFGPGKKGSLVVFAS 515
Cryptomys_hottentotus_mahali LLVIGTTLHVYPDLHSQFTYFQVLRVRLIKISPALEDFVYKIFGPGKKGSLVVFAS 515
Cryptomys_hottentotus_pretoriae LLVIGTTLHVYPDLHSQFTYFQVLRVRLIKISPALEDFVYKIFGPGKKGSLVVFAS 515
Cryptomys_hottentotus_natalensis LLVIGTTLHVYPDLHSQFTYFQVLRVRLIKISPALEDFVYKIFGPGKKGSLVVFAS 515
.~.*** *****

Danio_riero LLIVMSAISLQMFCEVLEDRFTTFPRAFMSMFQILTQEGWVDVMDQTLNAVGHMWAPVV 598
Marmota_marmota LLIVMSAISLQMFCEVLEDRFTTFPRAFMSMFQILTQEGWVDVMDQTLNAVGHMWAPVV 575
Tachyoryctes_splendens LLIVMSSISLQMFCEVLEDRFTTFPRAFMSMFQILTQEGWVDVMDQTLNAVGHMWAPVV 575
Rattus_norvegicus LLIVMSAISLQMFCEVLEDRFTTFPRAFMSMFQILTQEGWVDVMDQTLNAVGHMWAPLV 575
Mus_musculus LLIVMSAISLQMFCEVLEDRFTTFPRAFMSMFQILTQEGWVDVMDQTLNAVGHMWAPLV 575
Nannospalax_galili LLIVMSAISLQMFCEVLEDRFTTFPRAFMSMFQILTQEGWVDVMDQTLNAVGHMWAPVV 575
Homo_sapiens LLIVMSAISLQMFCEVLEDRFTTFPRAFMSMFQILTQEGWVDVMDQTLNAVGHMWAPVV 575
Pan_troglodytes LLIVMSAISLQMFCEVLEDRFTTFPRAFMSMFQILTQEGWVDVMDQTLNAVGHMWAPVV 575
Cavia_porcellus LLIVMSAISLQMFCEVLEDRFTTFPRAFMSMFQILTQEGWVDVMDQTLNAVGHMWAPVV 575
Heterocephalus_glaber LLIVMSAISLQMFCEVLEDRFTTFPRAFMSMFQILTQEGWVDVMDQTLNAVGHMWAPVV 575
Georchus_capensis LLIVMSAISLQMFCEVLEDRFTTFPRAFMSMFQILTQEGWVDVMDQTLNAVGHMWAPVV 575
Heliophobius_emini LLIVMSAISLQMFCEVLEDRFTTFPRAFMSMFQILTQEGWVDVMDQTLNAVGHMWAPVV 575
Fukomys_damarensis LLIVMSAISLQMFCEVLEDRFTTFPRAFMSMFQILTQEGWVDVMDQTLNAVGHMWAPVV 575
Cryptomys_hottentotus_hottentotus LLIVMSAISLQMFCEVLEDRFTTFPRAFMSMFQILTQEGWVDVMDQTLNAVGHMWAPVV 575
Cryptomys_hottentotus_mahali LLIVMSAISLQMFCEVLEDRFTTFPRAFMSMFQILTQEGWVDVMDQTLNAVGHMWAPVV 575
Cryptomys_hottentotus_pretoriae LLIVMSAISLQMFCEVLEDRFTTFPRAFMSMFQILTQEGWVDVMDQTLNAVGHMWAPVV 575
Cryptomys_hottentotus_natalensis LLIVMSAISLQMFCEVLEDRFTTFPRAFMSMFQILTQEGWVDVMDQTLNAVGHMWAPVV 575
*****.***~.*** *****

Danio_riero AIYFILYHLFATLILLSFVAVILDNLEDEDLKKLQKQSEANADTKEKPLRLRIFE 658
Marmota_marmota AIYFILYHLFATLILLSFVAVILDNLEDEDLKKLQKQSEANADTKEKPLRLRIFE 635
Tachyoryctes_splendens AIYFILYHLFATLILLSFVAVILDNLEDEDLKKLQKQSEANADTKEKPLRLRIFE 635
Rattus_norvegicus AIYFILYHLFATLILLSFVAVILDNLEDEDLKKLQKQSEANADTKEKPLRLRIFE 635
Mus_musculus AIYFILYHLFATLILLSFVAVILDNLEDEDLKKLQKQSEANADTKEKPLRLRIFE 635
Nannospalax_galili AIYFILYHLFATLILLSFVAVILDNLEDEDLKKLQKQSEANADTKEKPLRLRIFE 635
Homo_sapiens AIYFILYHLFATLILLSFVAVILDNLEDEDLKKLQKQSEANADTKEKPLRLRIFE 635
Pan_troglodytes AIYFILYHLFATLILLSFVAVILDNLEDEDLKKLQKQSEANADTKEKPLRLRIFE 635
Cavia_porcellus AIYFILYHLFATLILLSFVAVILDNLEDEDLKKLQKQSEANADTKEKPLRLRIFE 635
Heterocephalus_glaber AIYFILYHLFATLILLSFVAVILDNLEDEDLKKLQKQSEANADTKEKPLRLRIFE 635
Georchus_capensis AIYFILYHLFATLILLSFVAVILDNLEDEDLKKLQKQSEANADTKEKPLRLRIFE 635
Heliophobius_emini AIYFILYHLFATLILLSFVAVILDNLEDEDLKKLQKQSEANADTKEKPLRLRIFE 635
Fukomys_damarensis AIYFILYHLFATLILLSFVAVILDNLEDEDLKKLQKQSEANADTKEKPLRLRIFE 635
Cryptomys_hottentotus_hottentotus AIYFILYHLFATLILLSFVAVILDNLEDEDLKKLQKQSEANADTKEKPLRLRIFE 635
Cryptomys_hottentotus_mahali AIYFILYHLFATLILLSFVAVILDNLEDEDLKKLQKQSEANADTKEKPLRLRIFE 635
Cryptomys_hottentotus_pretoriae AIYFILYHLFATLILLSFVAVILDNLEDEDLKKLQKQSEANADTKEKPLRLRIFE 635
Cryptomys_hottentotus_natalensis AIYFILYHLFATLILLSFVAVILDNLEDEDLKKLQKQSEANADTKEKPLRLRIFE 635

Danio_riero KFPNRPQMVKISKLPDFTVPKIREFSMKQFIDRQQDTPSCLFRILPSASSSSCDHSKRS 718
Marmota_marmota KFPNRPQMVKISKLPDFTVPKIREFSMKQFIDRQQDTPSCLFRILPSASSSSCDHSKRS 695
Tachyoryctes_splendens KFPNRPQMVKISKLPDFTVPKIREFSMKQFIDRQQDTPSCLFRILPSASSSSCDHAKKA 695

Tachyoryctes splendens YHQLYDLLGLVLYLDWVMIIVTICSCISMMFESPFRRVMHPTLQIAEYVVFVIFMSIELN 934
Rattus norvegicus YHQLYDLLGLVLYLDWVMIIVTICSCISMMFESPFRRVMHPTLQIAEYVVFVIFMSIELN 934
Mus musculus YHQLYDLLGLVLYLDWVMIIVTICSCISMMFESPFRRVMHPTLQIAEYVVFVIFMSIELN 934
Nannospalax galili YHQLYDLLGLVLYLDWVMIIVTICSCISMMFESPFRRVMHPTLQIAEYVVFVIFMSIELN 935
Homo sapiens YHQLYDLLGLVLYLDWVMIIVTICSCISMMFESPFRRVMHPTLQIAEYVVFVIFMSIELN 934
Pan troglodytes YHQLYDLLGLVLYLDWVMIIVTICSCISMMFESPFRRVMHPTLQIAEYVVFVIFMSIELN 934
Cavia porcellus YHQLYDLLGLVLYLDWVMIIVTICSCISMMFESPFRRVMHPTLQIAEYVVFVIFMSIELN 934
Heterocephalus glaber YHQLYDLLGLVLYLDWVMIIVTICSCISMMFESPFRRVMHPTLQIAEYVVFVIFMSIELN 934
Georchus capensis YHQLYDLLGLVLYLDWVMIIVTICSCISMMFESPFRRVMHPTLQIAEYVVFVIFMSIELN 934
Heliophobius emini YHQLYDLLGLVLYLDWVMIIVTICSCISMMFESPFRRVMHPTLQIAEYVVFVIFMSIELN 934
Fukomys damarensis YHQLYDLLGLVLYLDWVMIIVTICSCISMMFESPFRRVMHPTLQIAEYVVFVIFMSIELN 934
Cryptomys hottentotus hottentotus YHQLYDLLGLVLYLDWVMIIVTICSCISMMFESPFRRVMHPTLQIAEYVVFVIFMSIELN 934
Cryptomys hottentotus mahali YHQLYDLLGLVLYLDWVMIIVTICSCISMMFESPFRRVMHPTLQIAEYVVFVIFMSIELN 934
Cryptomys hottentotus pretoriae YHQLYDLLGLVLYLDWVMIIVTICSCISMMFESPFRRVMHPTLQIAEYVVFVIFMSIELN 934
Cryptomys hottentotus natalensis YHQLYDLLGLVLYLDWVMIIVTICSCISMMFESPFRRVMHPTLQIAEYVVFVIFMSIELN 934

Danio rerio LKIMADGLFFPTAVIRDFGGVMDIFIVLSLIFLCWLPNNVPPESGAQLLMLRCLRPL 1017
Marmota marmota LKIMADGLFFPTAVIRDFGGVMDIFIVLSLIFLCWMPQNVPAESGAQLLMLRCLRPL 994
Tachyoryctes splendens LKIMADGLFFPTAVIRDFGGVMDIFIVLSLIFLCWMPQNVPPNSGAQLLMLRCLRPL 994
Rattus norvegicus LKIMADGLFFPTAVIRDFGGVMDIFIVLSLIFLCWMPQNVPAESGAQLLMLRCLRPL 994
Mus musculus LKIMADGLFFPTAVIRDFGGVMDIFIVLSLIFLCWMPQNVPAESGAQLLMLRCLRPL 994
Nannospalax galili LKIMADGLFFPTAVIRDFGGVMDIFIVLSLIFLCWMPQNVPAESGAQLLMLRCLRPL 995
Homo sapiens LKIMADGLFFPTAVIRDFGGVMDIFIVLSLIFLCWMPQNVPAESGAQLLMLRCLRPL 994
Pan troglodytes LKIMADGLFFPTAVIRDFGGVMDIFIVLSLIFLCWMPQNVPAESGAQLLMLRCLRPL 994
Cavia porcellus LKIMADGLFFPTAVIRDFGGVMDIFIVLSLIFLCWMPQNVPAESGAQLLMLRCLRPL 994
Heterocephalus glaber LKIMADGLFFPTAVIRDFGGVMDIFIVLSLIFLCWMPQNVPAESGAQLLMLRCLRPL 994
Georchus capensis LKIMADGLFFPTAVIRDFGGVMDIFIVLSLIFLCWMPQNVPAESGAQLLMLRCLRPL 994
Heliophobius emini LKIMADGLFFPTAVIRDFGGVMDIFIVLSLIFLCWMPQNVPAESGAQLLMLRCLRPL 994
Fukomys damarensis LKIMADGLFFPTAVIRDFGGVMDIFIVLSLIFLCWMPQNVPAESGAQLLMLRCLRPL 994
Cryptomys hottentotus hottentotus LKIMADGLFFPTAVIRDFGGVMDIFIVLSLIFLCWMPQNVRAESGAQLLMLRCLRPL 994
Cryptomys hottentotus mahali LKIMADGLFFPTAVIRDFGGVMDIFIVLSLIFLCWMPQNVRAESGAQLLMLRCLRPL 994
Cryptomys hottentotus pretoriae LKIMADGLFFPTAVIRDFGGVMDIFIVLSLIFLCWMPQNVRAESGAQLLMLRCLRPL 994
Cryptomys hottentotus natalensis LKIMADGLFFPTAVIRDFGGVMDIFIVLSLIFLCWMPQNVRAESGAQLLMLRCLRPL 994

Danio rerio RIFKLVPMQRKVVRELVKGFKEIFLVSILLTLMVLFATFGVQLFAGKLAKCNDPHISSK 1077
Marmota marmota RIFKLVPMQRKVVRELVKGFKEIFLVSILLTLMVLFASFGVQLFAGKLAKCNDPNIIR 1054
Tachyoryctes splendens RIFKLVPMQRKVVRELVKGFKEIFLVSILLTLMVLFASFGVQLFAGKLAKCNDPDIIRR 1054
Rattus norvegicus RIFKLVPMQRKVVRELVKGFKEIFLVSILLTLMVLFASFGVQLFAGKLAKCNDPNIIR 1054
Mus musculus RIFKLVPMQRKVVRELVKGFKEIFLVSILLTLMVLFASFGVQLFAGKLAKCNDPNIIR 1054
Nannospalax galili RIFKLVPMQRKVVRELVKGFKEIFLVSILLTLMVLFASFGVQLFAGKLAKCNDPYIIR 1055
Homo sapiens RIFKLVPMQRKVVRELVKGFKEIFLVSILLTLMVLFASFGVQLFAGKLAKCNDPNIIR 1054
Pan troglodytes RIFKLVPMQRKVVRELVKGFKEIFLVSILLTLMVLFASFGVQLFAGKLAKCNDPNIIR 1054
Cavia porcellus RIFKLVPMQRKVVRELVKGFKEIFLVSILLTLMVLFASFGVQLFAGKLAKCNDPNIIR 1054
Heterocephalus glaber RIFKLVPMQRKVVRELVKGFKEIFLVSILLTLMVLFASFGVQLFAGKLAKCNDPNIIR 1054
Georchus capensis RIFKLVPMQRKVVRELVKGFKEIFLVSILLTLMVLFASFGVQLFAGKLAKCNDPNIIR 1054
Heliophobius emini RIFKLVPMQRKVVRELVKGFKEIFLVSILLTLMVLFASFGVQLFAGKLAKCNDPNIIR 1054
Fukomys damarensis RIFKLVPMQRKVVRELVKGFKEIFLVSILLTLMVLFASFGVQLFAGKLAKCNDPNIIR 1054
Cryptomys hottentotus hottentotus RIFKLVPMQRKVVRELVKGFKEIFLVSILLTLMVLFASFGVQLFAGKLAKCNDPNIIR 1054
Cryptomys hottentotus mahali RIFKLVPMQRKVVRELVKGFKEIFLVSILLTLMVLFASFGVQLFAGKLAKCNDPNIIR 1054
Cryptomys hottentotus pretoriae RIFKLVPMQRKVVRELVKGFKEIFLVSILLTLMVLFASFGVQLFAGKLAKCNDPNIIR 1054
Cryptomys hottentotus natalensis RIFKLVPMQRKVVRELVKGFKEIFLVSILLTLMVLFASFGVQLFAGKLAKCNDPNIIR 1054

Danio rerio DDCHGIFRINVSISKNLNLKLRPGEKKPGFVWVPRVWVANPRNFNFDNVGNAMLALFEVLSL 1137
Marmota marmota EDCNGIFRINVSISKNLNLKLRPGEKKPGFVWVPRVWVANPRNFNFDNVGNAMLALFEVLSL 1114
Tachyoryctes splendens EDCHGIFRINVSISKNLNLKLRPGEKKPGFVWVPRVWVANPRNFNFDNVGNAMLALFEVLSL 1114
Rattus norvegicus EDCNGIFRINVSISKNLNLKLRPGEKKPGFVWVPRVWVANPRNFNFDNVGNAMLALFEVLSL 1114
Mus musculus EDCNGIFRINVSISKNLNLKLRPGEKKPGFVWVPRVWVANPRNFNFDNVGNAMLALFEVLSL 1114
Nannospalax galili EDCNGIFRINVSISKNLNLKLRPGEKKPGFVWVPRVWVANPRNFNFDNVGNAMLALFEVLSL 1115
Homo sapiens EDCNGIFRINVSISKNLNLKLRPGEKKPGFVWVPRVWVANPRNFNFDNVGNAMLALFEVLSL 1114
Pan troglodytes EDCNGIFRINVSISKNLNLKLRPGEKKPGFVWVPRVWVANPRNFNFDNVGNAMLALFEVLSL 1114
Cavia porcellus EDCNGIFRINVSISKNLNLKLRPGEKKPGFVWVPRVWVANPRNFNFDNVGNAMLALFEVLSL 1114
Heterocephalus glaber EDCNGIFRINVSISKNLNLKLRPGEKKPGFVWVPRVWVANPRNFNFDNVGNAMLALFEVLSL 1114
Georchus capensis EDCNGIFRINVSISKNLNLKLRPGEKKPGFVWVPRVWVANPRNFNFDNVGNAMLALFEVLSL 1114
Heliophobius emini EDCNGIFRINVSISKNLNLKLRPGEKKPGFVWVPRVWVANPRNFNFDNVGNAMLALFEVLSL 1114
Fukomys damarensis EDCNGIFRINVSISKNLNLKLRPGEKKPGFVWVPRVWVANPRNFNFDNVGNAMLALFEVLSL 1114
Cryptomys hottentotus hottentotus EDCSGIFRINVSISKNLNLKLRPGEKKPGFVWVPRVWVANPRNFNFDNVGNAMLALFEVLSL 1114
Cryptomys hottentotus mahali EDCSGIFRINVSISKNLNLKLRPGEKKPGFVWVPRVWVANPRNFNFDNVGNAMLALFEVLSL 1114
Cryptomys hottentotus pretoriae EDCSGIFRINVSISKNLNLKLRPGEKKPGFVWVPRVWVANPRNFNFDNVGNAMLALFEVLSL 1114
Cryptomys hottentotus natalensis EDCSGIFRINVSISKNLNLKLRPGEKKPGFVWVPRVWVANPRNFNFDNVGNAMLALFEVLSL 1114

Cryptomys_hottentotus_natalensis SMLSYSRVDIRKSLQLEELLAREQLEYTIEEEVAKQTIRMWLKCLKRIRAKQQQCSII 1590

Danio_riero LSLRESQQQLRR-LLNPPSIETTVPS EDTNTHNQDNPTQPENSGLQTL SPTLSDRSGY 1676
 Marmota_marmota HSLRESQQQLSR-FLNPPSIETTQPS EDTTANSQDPNMPPTSSQQQLSPTLSDRGGG 1649
 Tachyoryctes_splendens HSLRESQQQLSR-FLNPPSIETTQPS EDTNANSQDHNAPPETSSQQQLSPTLSDRGGG 1649
 Rattus_norvegicus HSLRESQQQLSR-FLNPPSIETTQPS EDTNANSQDHNTPPESSQQQLSPTLSDRGGG 1648
 Mus_musculus HSLRESQQQLSR-FLNPPSIETTQPS EDTNANSQDHSMQPETSSQQQLSPTLSDRGGG 1650
 Nannospalax_galili HSLRESQQQLSR-FLNPPSIETTQPS EDTANSQDHNTPPETSSQQQLSPTLSDRGGG 1650
 Homo_sapiens HSLRESQQQLSR-FLNPPSIETTQPS EDTNANSQDHSMQPETSSQQQLSPTLSDRGGG 1653
 Pan_troglodytes HSLRESQQQLSR-FLNPPSIETTQPS EDTNANSQDHSMQPETSSQQQLSPTLSDRGGG 1653
 Cavia_porcellus HSLRESQQQLSR-FLNPPSIETTQPS EDTNANSQDHNTPPETSSQQQLSPTLSDRGGG 1649
 Heterocephalus_glaber HSLRESQQQLSR-FLNPPSIETTQPS EDTNASSQDHNMQPETSSQQQLSPTLSDRGGG 1649
 Georchus_capensis HSLRESQQQLSR-FLNPPSIETTQPS EDTNASSQDHNMQPETSSQQQLSPTLSDRGGG 1649
 Heliophobius_emini HSLRESQQQLSR-FLNPPSIETTQPS EDTNASSQDHSMQPETSSQQQLSPTLSDRGGG 1649
 Fukomys_damarensis HSLRESQQQLSR-FLNPPSIETTQPS EDTNASSQDHNMQPETSSQQQLSPTLSDRGGG 1649
 Cryptomys_hottentotus_hottentotus HSLRESQQQLSR-FLNPPSIETTQPS EDTNASSQDHNMQPETSSQQQLSPTLSDRGGG 1649
 Cryptomys_hottentotus_mahali HSLRESQQQLSR-FLNPPSIETTQPS EDTNASSQDHNMQPETSSQQQLSPTLSDRGGG 1649
 Cryptomys_hottentotus_pretoriae HSLRESQQQLSR-FLNPPSIETTQPS EDTNASSQDHNMQPETSSQQQLSPTLSDRGGG 1649
 Cryptomys_hottentotus_natalensis HSLRESQQQLSR-FLNPPSIETTQPS EDTNASSQDHNMQPETSSQQQLSPTLSDRGGG 1649
 *****: * ..***** ** ..* ..***** *

Danio_riero RQDSA--DRPQRKLGQWRLPA-----GRTSVKSMVCKMNPVTEASSG 1717
 Marmota_marmota RQDASEAEKPKRQKVGQWCRPSDPSLSQLP PAVTFPCGERIKMKS VVCKMNPVTAASSG 1709
 Tachyoryctes_splendens RQDAADPGKPKRQKFGQWRLPSAPK PISHSVSSVNLRFGGRTTMKS VVCKMNPMPDTASSG 1709
 Rattus_norvegicus RQDAADTGKPKRQKIGQWRLPSAPK PISHSVSSVNLRFGGRTTMKS VVCKMNPMPDTASSG 1708
 Mus_musculus RQDAADTGKPKRQKIGQWRLPSAPK PISHSVSSVNLRFGGRTTMKTVVCKMNPMPDTASSG 1710
 Nannospalax_galili RQDAADPGKPKRQKFGQWRLPSAPK PISHSVSSVNLRFGGRTTMKS VVCKMNPMPDTASSG 1710
 Homo_sapiens RQDAADAGKPKRQKFGQWRLPSAPK PISHSVSSVNLRFGGRTTMKS VVCKMNPMTDAASSG 1713
 Pan_troglodytes RQDAADAGKPKRQKFGQWRLPSAPK PISHSVSSVNLRFGGRTTMKS VVCKMNPMTDAASSG 1713
 Cavia_porcellus RQDAGDAGKPKRQKFGQWRLPSAPK PISHSVSSVNLRFGGRTTMKS VVCKMNPMTDAASSG 1709
 Heterocephalus_glaber RQDTGDAGKPKRQKFGQWRLPSAPK PISHSVSSVNLRFGGRTTMKS VVCKVSPMTDAASSG 1709
 Georchus_capensis RQDTGDAGKPKRQKFGQWRLPSAPK PISHSVSSVNLRFGGRTTMKS VVCKMNPMTDAASSG 1709
 Heliophobius_emini RQDTGDAGKPKRQKFGQWRLPSAPK PISHSVSSVNLRFGGRTTMKS VVCKMNPMTDAASSG 1709
 Fukomys_damarensis RQDTGDAGKPKRQKFGQWRLPSAPK PISHSVSSVNLRFGGRTTMKS VVCKMNPMTDAASSG 1709
 Cryptomys_hottentotus_hottentotus RQDTGDAGKPKRQKFGQWRLPSAPK PISHSVSSVNLRFGGRTTMKS VVCKMNPMTDAASSG 1709
 Cryptomys_hottentotus_mahali RQDTGDAGKPKRQKFGQWRLPSAPK PISHSVSSVNLRFGGRTTMKS VVCKMNPMTDAASSG 1709
 Cryptomys_hottentotus_pretoriae RQDTGDAGKPKRQKFGQWRLPSAPK PISHSVSSVNLRFGGRTTMKS VVCKMNPMTDAASSG 1709
 Cryptomys_hottentotus_natalensis RQDTGDAGKPKRQKFGQWRLPSAPK PISHSVSSVNLRFGGRTTMKS VVCKMNPMTDAASSG 1709
 * ..***** * : * ..***** * ..***** *

Danio_riero SEVKKWWTRQLTVESDES GDDLIDI 1742
 Marmota_marmota SEVKKWWTRQLTVESDES GDDLIDV 1734
 Tachyoryctes_splendens SEVKKWWTRQLTVESDES GDDLIDL 1734
 Rattus_norvegicus SEVKKWWTRQLTVESDES GDDLIDI 1733
 Mus_musculus SEVKKWWTRQLTVESDES GDDLIDI 1735
 Nannospalax_galili SEVKKWWTRQLTVESDES GDDLIDI 1735
 Homo_sapiens SEVKKWWTRQLTVESDES GDDLIDI 1738
 Pan_troglodytes SEVKKWWTRQLTVESDES GDDLIDI 1738
 Cavia_porcellus SEVKKWWTRQLTVESDES GDDLIDI 1734
 Heterocephalus_glaber SEVKKWWTRQLTVESDES EDDLIDI 1734
 Georchus_capensis SEVKKWWTRQLTVESDES GDDLIDI 1734
 Heliophobius_emini SEVKKWWTRQLTVESDES GDDLIDI 1734
 Fukomys_damarensis SEVKKWWTRQLTVESDES GDDLIDI 1734
 Cryptomys_hottentotus_hottentotus SEVKKWWTRQLTVESDES GDDLIDI 1734
 Cryptomys_hottentotus_mahali SEVKKWWTRQLTVESDES GDDLIDI 1734
 Cryptomys_hottentotus_pretoriae SEVKKWWTRQLTVESDES GDDLIDI 1734
 Cryptomys_hottentotus_natalensis SEVKKWWTRQLTVESDES GDDLIDI 1734
 *****: ..***** * ..***** *

Fig. S7

NALCN alignment, Alignment of NALCN amino acid sequences from *Cryptomys* species against a range of NALCN sequences across the animal kingdom.

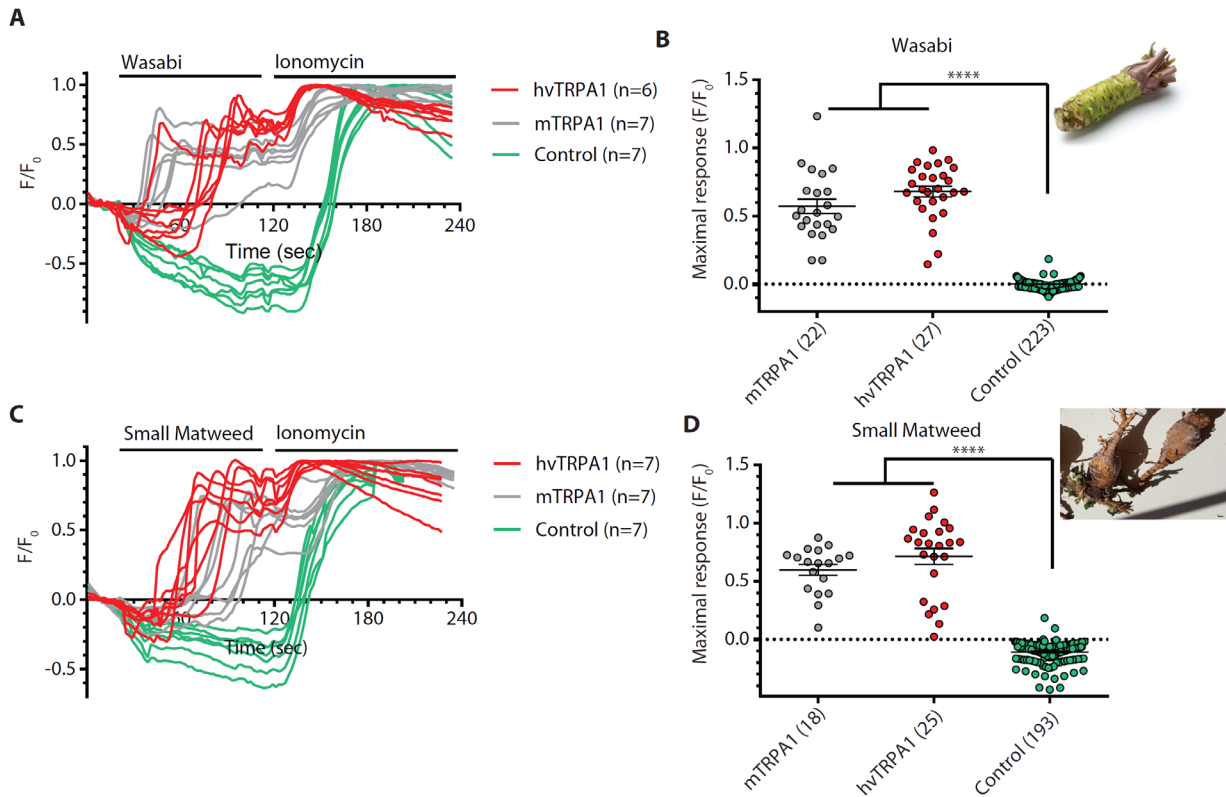


Fig. S8

Root extracts activate TRPA1 A) Representative calcium traces after application of a 10% (w/v) wasabi extract solution on HEK293 cells expressing TRPA1 from mouse (m) or Highveld mole-rats (hv). Every trace represents the data from 1 cell (n). B) Maximal fluorescence intensity was measured after application of the wasabi solution on the cells (n=number of cells from 3 different coverslips) (error bars indicate SEM; **** $P \leq 0.0001$; Unpaired t test). C) and D) show the same for the Small matweed extract indicating there is a TRPA1 activating substance in plants found in the natural habitat of the Highveld mole-rat. Note that the calcium responses were as large as the ionomycin control indicating that TRPA1 channels were probably maximally activated with the concentration of the ligand found in the extract.

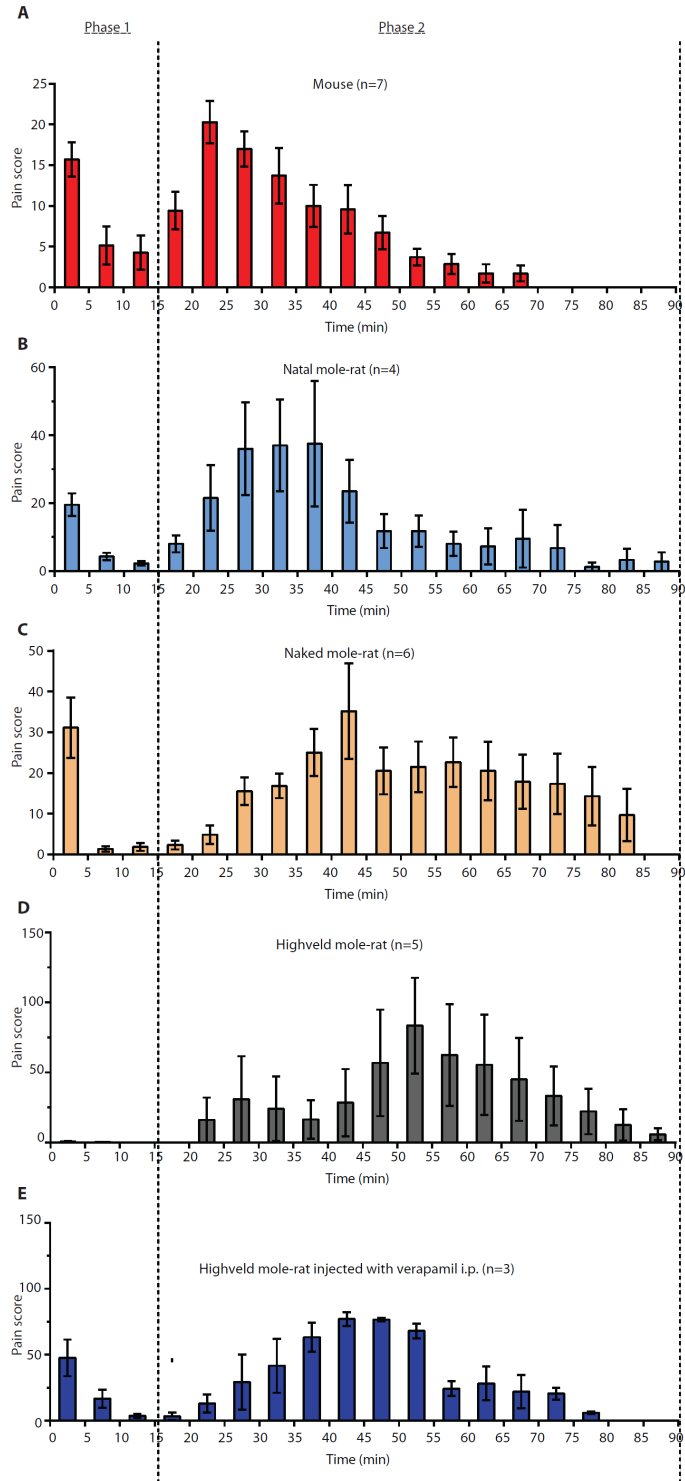


Fig. S9
Formalin Test in different African mole-rats. Frequency of pain behaviors after an injection of 2% Formalin into the paw. Phase 1 was defined as the response from 0-15 minutes, phase 2 from 15-90 minutes. Note that the magnitude of the pain behavior does vary across species but the time course of the response was very similar across species with the notable exception of the Highveld mole-rat.

Species	Number	Sex	Age/weight	Tissue sample	#read pairs	De novo assembly	Expression analysis
Mouse <i>Mus musculus</i>	M1	m	8 months	DRG, SC	188,962,096	no	yes
	M2	m	8 months	DRG, SC			
	M3	m	8 months	DRG, SC			
East African root rat <i>Tachyoryctes splendens</i>	RR1	m	380.8g	DRG, SC	211,112,254	yes	yes
	RR2	m	439.0g	DRG, SC			
	RR4	m	439.0g	DRG, SC			
Naked mole-rat <i>Heterocephalus glaber</i>	NMR1	m	6 years	SC	188,470,734	no	yes
	NMR2	m	6 years	SC			
	NMR3	m	6 years	SC			
	NMR1.2	m	59.2g	DRG			
	NMR2.2	m	70.4g	DRG			
	NMR3.2	m	56.6g	DRG			
Emin's mole-rat <i>Heliophobius emini</i>	He5	m	60g	DRG	187,929,353	yes	no
	He14	m	ND	DRG			
	He3.2	m	ND	Muscle			
	He5.2	m	ND	Brain			
	He7	m	ND	TGG			
Cape mole-rat <i>Georychus capensis</i>	G1	f	100.8g	DRG, SC	172,818,386	yes	yes
	G2	f	147.0g	DRG, SC			
	G3	f	138.7g	DRG, SC			
Common mole-rat <i>Cryptomys hottentotus hottentotus</i>	HH3	f	35.6g	DRG, SC	156,707,245	yes	yes
	HH4	f	40.3g	DRG, SC			
	HH5	f	47.1g	DRG, SC			
Mahali mole-rat <i>Cryptomys hottentotus mahali</i>	Ma8	m	125g	DRG, SC	229,281,786	yes	no
	Ma9	f	99.4g	DRG, SC			
	Ma10	f	57.5g	DRG, SC			
Natal mole-rat <i>Cryptomys hottentotus natalensis</i>	N1	f	72.0g	DRG, SC	181,402,359	yes	yes
	N2	f	74.0g	SC			
	N3	f	99.8g	DRG, SC			
Highveld mole-rat <i>Cryptomys hottentotus pretoriae</i>	P1	f	84.3g	DRG, SC	194,791,919	yes	yes
	P2	f	90.0g	DRG, SC			
	P3	f	143.6g	SC			
	P4	f	85.5g	DRG			
Damaraland mole-rat <i>Fukomys damarensis</i>	D1	m	70.3g	DRG, SC	181,073,339	no	yes
	D2	f	54.6g	DRG, SC			
	D3	f	57.0g	DRG, SC			

Table S1: Overview of tissues and species used for transcriptome analysis. Sex, weight/age and sequencing depth summed up per species. For most species, these reads were used for de novo transcriptome assembly and transcript quantification. m= male, f=female, dorsal root ganglia (DRG, Spinal cord (SC), Not determined (ND). Sequencing reads were deposited at the NCBI Sequencing Read Archive under accession number PRJNA394865.

species	# full-length protein-coding transcripts	BUSCO score
<i>Tachyoryctes splendens</i>	10,786	76 %
<i>Heliophobius emini</i>	9,553	70 %
<i>Georychus capensis</i>	9,678	71 %
<i>Cryptomys hottentotus hottentotus</i>	9,521	69 %
<i>Cryptomys hottentotus mahali</i>	9,630	70 %
<i>Cryptomys hottentotus natalensis</i>	9,691	70 %
<i>Cryptomys hottentotus pretoriae</i>	9,531	69 %

Table S2 Statistics for de novo transcriptome assemblies. The number of full-length protein-coding transcripts and completeness scores per species for the de novo assembled and annotated transcriptomes.

Capsaicin-insensitive against background

gene name	description	F-value	logFC	p.adj
BMPER	BMP-binding endothelial regulator	42.58	-1.1	0.005333

Acid-insensitive against background

gene name	description	F-value	logFC	p.adj
CROT	carnitine O-octanoyltransferase	44.94	-1.85	0.003654
ANKMY2	ankyrin repeat and MYND domain containing 2	46.93	1.41	0.003654
RGS10	regulator of G-protein signalling 10	41.52	-2.49	0.004759
PHF24	PHD finger protein 24	36.38	-1.44	0.005969
DDX56	DEAD (Asp-Glu-Ala-Asp) box polypeptide 56	33.46	-1.16	0.008914
PTPN5	protein tyrosine phosphatase, non-receptor type 5	31.5	3.64	0.0111
WBSCR22	Williams Beuren syndrome chromosome region 22	30.67	1.04	0.0111
UFSP2	UFM1-specific peptidase 2	28.74	-1.29	0.01297
HMCES	5-hydroxymethylcytosine (hmC) binding, ES cell specific	29.01	1.11	0.01297
IMPDH2	inosine 5'-phosphate dehydrogenase 2	27.61	1.01	0.01554
SLC25A30	solute carrier family 25, member 30	26.93	-2.8	0.01613
SLC46A1	solute carrier family 46, member 1	27.07	2.12	0.01613
PLXNC1	plexin C1	25.6	-2.15	0.01694
DOCK11	dedicator of cytokinesis 11	25.48	-1.06	0.01694
FAAP24	Fanconi anemia core complex associated protein 24	24.88	1.2	0.01817
EPB41L4A	erythrocyte membrane protein band 4.1 like 4a	24.36	1.62	0.01898
SPR	sepiapterin reductase	24.06	-1.48	0.01898
STAMBPL1	STAM binding protein like 1	23.65	1.6	0.01971
RAB40B	Rab40B, member RAS oncogene family	23.13	1.48	0.01994
PAQR7	progesterin and adipoQ receptor family member VII	23.09	-1.43	0.01994
RNASEH2A	ribonuclease H2, large subunit	23.18	-1.14	0.01994
PEX11G	peroxisomal biogenesis factor 11 gamma	22.88	1.19	0.02
CABLES2	CDK5 and Abl enzyme substrate 2	22.08	1.46	0.02156
ANGEL2	angel homolog 2	22.08	-1.02	0.02156
PTGFR	prostaglandin F receptor	21.57	-1.35	0.02254
TRAF3IP2	TRAF3 interacting protein 2	21.55	1.26	0.02254
ALDH9A1	aldehyde dehydrogenase 9, subfamily A1	21.64	-1.18	0.02254
TCTEX1D2	Tctex1 domain containing 2	21.71	1.1	0.02254
DMAP1	DNA methyltransferase 1-associated protein 1	21.39	1.03	0.02294
GRHPR	glyoxylate reductase/hydroxypyruvate reductase	21.18	1.62	0.02328
RGMA	repulsive guidance molecule family member A	21.25	1.4	0.02328
KCNK1	potassium channel, subfamily K, member 1	20.79	-1.05	0.02462
MED6	mediator complex subunit 6	19.83	1.03	0.0285
CBS	cystathionine beta-synthase	19.26	3.25	0.032
HSD17B7	hydroxysteroid (17-beta) dehydrogenase 7	19.18	-1.21	0.03216
RTKN	rhotekin	18.6	1.22	0.03643
SLC25A48	solute carrier family 25, member 48	18.37	4.15	0.03755
ASIC3	acid-sensing (proton-gated) ion channel 3	18.17	-1.67	0.03859
SLC50A1	solute carrier family 50 (sugar transporter), member 1	17.61	-1	0.04368
PXMP4	peroxisomal membrane protein 4	17.54	-1.34	0.04389
ZBTB6	zinc finger and BTB domain containing 6	17.21	-1.36	0.04745

AITC-insensitive against background

gene name	description	F-value	logFC	p.adj
NALCN	sodium leak channel, non-selective	37.49	2.81	0.03806

Table S3 Differentially expressed genes found in the DRG. Statistical details for all significantly differentially regulated the genes. Data is shown for genes found to be differentially regulated in capsaicin insensitive (top), acid insensitive (middle) and AITC-insensitive species. Transcripts are sorted by adjusted p-value and log fold change.

gene name	description	LR	qval	# sites	ω_2	ω_3
ANO3	anoctamin 3	43.11	8.79e-08	3	0.234	1.280
ATP8B1	ATPase, class I, type 8B, member 1	39.78	3.58e-07	1	0.202	0.962
MAN2B1	mannosidase 2, alpha B1	39.37	3.58e-07	14	0.245	0.965
ST8SIA3	ST8 alpha-N-acetyl-neuraminide alpha-2,8-sialyltransferase 3	32.87	7.17e-06	2	0.104	5.715
MAN2A2	mannosidase 2, alpha 2	32.15	9.10e-06	3	0.232	1.144
CXCR4	chemokine (C-X-C motif) receptor 4	28.86	3.61e-05	2	0.167	1.722
MGAT4C	MGAT4 family, member C	23.57	5.11e-04	1	0.126	0.900
ROPN1L	ropporin 1-like	22.98	5.99e-04	6	0.513	6.411
PLAC8	placenta-specific 8	22.62	6.71e-04	2	0.220	12.375
ANO5	anoctamin 5	22.26	7.16e-04	10	0.248	0.890
HTRA2	HtrA serine peptidase 2	21.62	8.76e-04	1	0.170	3.038
NFE2L2	nuclear factor, erythroid derived 2, like 2	21.56	8.76e-04	1	0.262	26.869
FAM168A	family with sequence similarity 168, member A	21.22	9.95e-04	1	0.035	17.700
NLRX1	NLR family member X1	20.93	1.11e-03	2	0.291	1.260
NXPE3	neurexophilin and PC-esterase domain family, member 3	19.51	1.97e-03	3	0.299	1.953
ADAMTS1	a disintegrin-like and metallopeptidase (reprolysin type) with thrombospondin type 1 motif, 1	19.22	2.13e-03	6	0.285	0.886
ANO10	anoctamin 10	18.88	2.36e-03	1	0.194	0.616
POGLUT1	protein O-glucosyltransferase 1	18.04	3.16e-03	1	0.183	43.862
SYTL5	synaptotagmin-like 5	18.06	3.16e-03	3	0.345	2.920
QPCTL	glutaminy-peptide cyclotransferase-like	17.04	4.90e-03	1	0.281	1.598
DNAJB2	DnaJ heat shock protein family (Hsp40) member B2	17.00	4.90e-03	2	0.357	2.451
IFT57	intraflagellar transport 57	16.85	4.94e-03	1	0.016	0.233
RET	ret proto-oncogene	16.84	4.94e-03	7	0.232	0.568
ZBTB33	zinc finger and BTB domain containing 33	15.80	7.66e-03	1	0.351	1.142
UBE3A	ubiquitin protein ligase E3A	15.38	8.98e-03	1	0.188	1.748
FAM57B	family with sequence similarity 57, member B	15.10	9.65e-03	1	0.325	8.273
SPRED2	sprouty-related, EVH1 domain containing 2	15.10	9.65e-03	1	0.146	1.232
DAGLB	diacylglycerol lipase, beta	14.41	1.32e-02	13	0.385	1.141
SLC44A2	solute carrier family 44, member 2	13.98	1.52e-02	1	0.233	0.832
SLC7A8	solute carrier family 7 (cationic amino acid transporter, y+ system), member 8	13.69	1.63e-02	1	0.224	115.042
FURIN*	furin (paired basic amino acid cleaving enzyme)	13.40	1.86e-02	2	0.460	0.000
CERK	ceramide kinase	13.14	2.11e-02	5	0.203	0.768
CNKSR3	Cnksr family member 3	12.57	2.67e-02	1	0.187	0.798
ALKBH4	alkB homolog 4, lysine demethylase	12.37	2.83e-02	3	0.160	1.327
LRRCC1	leucine rich repeat and coiled-coil domain containing 1	12.39	2.83e-02	4	0.260	2.621
FGG	fibrinogen gamma chain	12.32	2.86e-02	2	0.293	0.956
NDUFV1	NADH dehydrogenase (ubiquinone) flavoprotein 1	11.93	3.31e-02	1	0.098	0.459
QSOX2	quiescin Q6 sulfhydryl oxidase 2	11.96	3.31e-02	11	0.305	0.945
MANEA	mannosidase, endo-alpha	11.87	3.40e-02	3	0.282	0.886
IMMT	inner membrane protein, mitochondrial	11.81	3.47e-02	2	0.487	2.798
TXNDC15	thioredoxin domain containing 15	11.46	4.04e-02	1	0.238	1.107
PARS2	prolyl-tRNA synthetase (mitochondrial)(putative)	11.21	4.33e-02	1	0.338	1.196
FAM193B	family with sequence similarity 193, member B	11.06	4.65e-02	1	0.837	2.318

Table S4 Divergent selection in the acid-insensitive East African root rat. Genes under divergent selection in the east African root rat (*Tachyoryctes splendens*). LR (likelihood ratio)

indicates the signal strength of the divergent selection model. Genes are sorted by adjusted p-value. # sites reports the number of amino acids under divergent selection pressure. ω_2 (background) and ω_3 (foreground) depict the non-synonymous to synonymous substitution rates. $\omega_2 < \omega_3$ indicates negative selection, $\omega_2 > \omega_3$ implies positive selection. FURIN as the only gene under negative selection is highlighted with an asterisk.

Movie S1

Movie showing positive nocifensive behaviors in African Rodent Species that lack a response to one of the three algogens used. For each species one video is shown with an algogen that provokes behavior and one that does not.

References and Notes

1. A. H. Rowe, Y. Xiao, M. P. Rowe, T. R. Cummins, H. H. Zakon, Voltage-gated sodium channel in grasshopper mice defends against bark scorpion toxin. *Science* **342**, 441–446 (2013). [doi:10.1126/science.1236451](https://doi.org/10.1126/science.1236451) [Medline](#)
2. C. J. Bohlen, A. T. Chesler, R. Sharif-Naeini, K. F. Medzihradsky, S. Zhou, D. King, E. E. Sánchez, A. L. Burlingame, A. I. Basbaum, D. Julius, A heteromeric Texas coral snake toxin targets acid-sensing ion channels to produce pain. *Nature* **479**, 410–414 (2011). [doi:10.1038/nature10607](https://doi.org/10.1038/nature10607) [Medline](#)
3. J. Van Hees, J. Gybels, C nociceptor activity in human nerve during painful and non painful skin stimulation. *J. Neurol. Neurosurg. Psychiatry* **44**, 600–607 (1981). [doi:10.1136/jnnp.44.7.600](https://doi.org/10.1136/jnnp.44.7.600) [Medline](#)
4. M. J. Caterina, M. A. Schumacher, M. Tominaga, T. A. Rosen, J. D. Levine, D. Julius, The capsaicin receptor: A heat-activated ion channel in the pain pathway. *Nature* **389**, 816–824 (1997). [doi:10.1038/39807](https://doi.org/10.1038/39807) [Medline](#)
5. S.-E. Jordt, D. M. Bautista, H. H. Chuang, D. D. McKemy, P. M. Zygmunt, E. D. Högestätt, I. D. Meng, D. Julius, Mustard oils and cannabinoids excite sensory nerve fibres through the TRP channel ANKTM1. *Nature* **427**, 260–265 (2004). [doi:10.1038/nature02282](https://doi.org/10.1038/nature02282) [Medline](#)
6. G. M. Story, A. M. Peier, A. J. Reeve, S. R. Eid, J. Mosbacher, T. R. Hricik, T. J. Earley, A. C. Hergarden, D. A. Andersson, S. W. Hwang, P. McIntyre, T. Jegla, S. Bevan, A. Patapoutian, ANKTM1, a TRP-like channel expressed in nociceptive neurons, is activated by cold temperatures. *Cell* **112**, 819–829 (2003). [doi:10.1016/S0092-8674\(03\)00158-2](https://doi.org/10.1016/S0092-8674(03)00158-2) [Medline](#)
7. E. S. J. Smith, G. R. Lewin, Nociceptors: A phylogenetic view. *J. Comp. Physiol. A Neuroethol. Sens. Neural Behav. Physiol.* **195**, 1089–1106 (2009). [doi:10.1007/s00359-009-0482-z](https://doi.org/10.1007/s00359-009-0482-z) [Medline](#)
8. E. S. J. Smith, D. Omerbašić, S. G. Lechner, G. Anirudhan, L. Lapatsina, G. R. Lewin, The molecular basis of acid insensitivity in the African naked mole-rat. *Science* **334**, 1557–1560 (2011). [doi:10.1126/science.1213760](https://doi.org/10.1126/science.1213760) [Medline](#)
9. T. J. Park, Y. Lu, R. Jüttner, E. S. J. Smith, J. Hu, A. Brand, C. Wetzel, N. Milenkovic, B. Erdmann, P. A. Heppenstall, C. E. Laurito, S. P. Wilson, G. R. Lewin, Selective inflammatory pain insensitivity in the African naked mole-rat (*Heterocephalus glaber*). *PLOS Biol.* **6**, e13 (2008). [doi:10.1371/journal.pbio.0060013](https://doi.org/10.1371/journal.pbio.0060013) [Medline](#)
10. D. A. Simone, T. K. Baumann, R. H. LaMotte, Dose-dependent pain and mechanical hyperalgesia in humans after intradermal injection of capsaicin. *Pain* **38**, 99–107 (1989). [doi:10.1016/0304-3959\(89\)90079-1](https://doi.org/10.1016/0304-3959(89)90079-1) [Medline](#)
11. K. H. Steen, U. Issberner, P. W. Reeh, Pain due to experimental acidosis in human skin: Evidence for non-adapting nociceptor excitation. *Neurosci. Lett.* **199**, 29–32 (1995). [doi:10.1016/0304-3940\(95\)12002-L](https://doi.org/10.1016/0304-3940(95)12002-L) [Medline](#)
12. N. C. Bennett, C. G. Faulkes, *African Mole-Rats: Ecology and Eusociality* (Cambridge Univ. Press, 2000).

13. C. G. Faulkes, N. C. Bennett, F. P. D. Cotterill, W. Stanley, G. F. Mgone, E. Verheyen, Phylogeography and cryptic diversity of the solitary-dwelling silvery mole-rat, genus *Heliophobius* (family: Bathyergidae). *J. Zool.* **285**, 324–338 (2011). [doi:10.1111/j.1469-7998.2011.00863.x](https://doi.org/10.1111/j.1469-7998.2011.00863.x)
14. B. D. Patterson, N. S. Upham, A newly recognized family from the Horn of Africa, the Heterocephalidae (Rodentia: Ctenohystrica). *Zool. J. Linn. Soc.* **172**, 942–963 (2014). [doi:10.1111/zoj.12201](https://doi.org/10.1111/zoj.12201)
15. T. J. Park, J. Reznick, B. L. Peterson, G. Blass, D. Omerbašić, N. C. Bennett, P. H. J. L. Kuich, C. Zasada, B. M. Browe, W. Hamann, D. T. Applegate, M. H. Radke, T. Kosten, H. Lutermann, V. Gavaghan, O. Eigenbrod, V. Bégay, V. G. Amoroso, V. Govind, R. D. Minshall, E. S. J. Smith, J. Larson, M. Gotthardt, S. Kempa, G. R. Lewin, Fructose-driven glycolysis supports anoxia resistance in the naked mole-rat. *Science* **356**, 307–311 (2017). [doi:10.1126/science.aab3896](https://doi.org/10.1126/science.aab3896) [Medline](#)
16. Z. Chang, G. Li, J. Liu, Y. Zhang, C. Ashby, D. Liu, C. L. Cramer, X. Huang, Bridger: A new framework for de novo transcriptome assembly using RNA-seq data. *Genome Biol.* **16**, 30 (2015). [doi:10.1186/s13059-015-0596-2](https://doi.org/10.1186/s13059-015-0596-2) [Medline](#)
17. M. G. Grabherr, B. J. Haas, M. Yassour, J. Z. Levin, D. A. Thompson, I. Amit, X. Adiconis, L. Fan, R. Raychowdhury, Q. Zeng, Z. Chen, E. Mauceli, N. Hacohen, A. Gnirke, N. Rhind, F. di Palma, B. W. Birren, C. Nusbaum, K. Lindblad-Toh, N. Friedman, A. Regev, Full-length transcriptome assembly from RNA-seq data without a reference genome. *Nat. Biotechnol.* **29**, 644–652 (2011). [doi:10.1038/nbt.1883](https://doi.org/10.1038/nbt.1883) [Medline](#)
18. K. T. J. Davies, N. C. Bennett, G. Tsagkogeorga, S. J. Rossiter, C. G. Faulkes, Family wide molecular adaptations to underground life in African mole-rats revealed by phylogenomic analysis. *Mol. Biol. Evol.* **32**, 3089–3107 (2015). [Medline](#)
19. D. Usoskin, A. Furlan, S. Islam, H. Abdo, P. Lönnerberg, D. Lou, J. Hjerling-Leffler, J. Haeggström, O. Kharchenko, P. V. Kharchenko, S. Linnarsson, P. Ernfors, Unbiased classification of sensory neuron types by large-scale single-cell RNA sequencing. *Nat. Neurosci.* **18**, 145–153 (2015). [doi:10.1038/nn.3881](https://doi.org/10.1038/nn.3881) [Medline](#)
20. N. Milenkovic, C. Frahm, M. Gassmann, C. Griffel, B. Erdmann, C. Birchmeier, G. R. Lewin, A. N. Garratt, Nociceptive tuning by stem cell factor/c-Kit signaling. *Neuron* **56**, 893–906 (2007). [doi:10.1016/j.neuron.2007.10.040](https://doi.org/10.1016/j.neuron.2007.10.040) [Medline](#)
21. F. Lesage, E. Guillemare, M. Fink, F. Duprat, M. Lazdunski, G. Romey, J. Barhanin, TWIK-1, a ubiquitous human weakly inward rectifying K⁺ channel with a novel structure. *EMBO J.* **15**, 1004–1011 (1996). [doi:10.1002/j.1460-2075.1996.tb00437.x](https://doi.org/10.1002/j.1460-2075.1996.tb00437.x) [Medline](#)
22. R. Waldmann, F. Bassilana, J. de Weille, G. Champigny, C. Heurteaux, M. Lazdunski, Molecular cloning of a non-inactivating proton-gated Na⁺ channel specific for sensory neurons. *J. Biol. Chem.* **272**, 20975–20978 (1997). [doi:10.1074/jbc.272.34.20975](https://doi.org/10.1074/jbc.272.34.20975) [Medline](#)
23. M. P. Price, S. L. McIlwrath, J. Xie, C. Cheng, J. Qiao, D. E. Tarr, K. A. Sluka, T. J. Brennan, G. R. Lewin, M. J. Welsh, The DRASIC cation channel contributes to the detection of cutaneous touch and acid stimuli in mice. *Neuron* **32**, 1071–1083 (2001). [doi:10.1016/S0896-6273\(01\)00547-5](https://doi.org/10.1016/S0896-6273(01)00547-5) [Medline](#)

24. L.-N. Schuhmacher, G. Callejo, S. Srivats, E. S. J. Smith, Naked mole-rat acid-sensing ion channel 3 forms nonfunctional homomers, but functional heteromers. *J. Biol. Chem.* **293**, 1756–1766 (2018). [doi:10.1074/jbc.M117.807859](https://doi.org/10.1074/jbc.M117.807859) [Medline](#)
25. F. C. Chatelain, D. Bichet, D. Douguet, S. Feliciangeli, S. Bendahhou, M. Reichold, R. Warth, J. Barhanin, F. Lesage, TWIK1, a unique background channel with variable ion selectivity. *Proc. Natl. Acad. Sci. U.S.A.* **109**, 5499–5504 (2012). [doi:10.1073/pnas.1201132109](https://doi.org/10.1073/pnas.1201132109) [Medline](#)
26. A. Latremoliere, A. Latini, N. Andrews, S. J. Cronin, M. Fujita, K. Gorska, R. Hovius, C. Romero, S. Chuaiphichai, M. Painter, G. Miracca, O. Babaniyi, A. P. Remor, K. Duong, P. Riva, L. B. Barrett, N. Ferreirós, A. Naylor, J. M. Penninger, I. Tegeder, J. Zhong, J. Blagg, K. M. Channon, K. Johnsson, M. Costigan, C. J. Woolf, Reduction of neuropathic and inflammatory pain through inhibition of the tetrahydrobiopterin pathway. *Neuron* **86**, 1393–1406 (2015). [doi:10.1016/j.neuron.2015.05.033](https://doi.org/10.1016/j.neuron.2015.05.033) [Medline](#)
27. B. Lu, Y. Su, S. Das, J. Liu, J. Xia, D. Ren, The neuronal channel NALCN contributes resting sodium permeability and is required for normal respiratory rhythm. *Cell* **129**, 371–383 (2007). [doi:10.1016/j.cell.2007.02.041](https://doi.org/10.1016/j.cell.2007.02.041) [Medline](#)
28. D. Omerbašić, E. S. J. Smith, M. Moroni, J. Homfeld, O. Eigenbrod, N. C. Bennett, J. Reznick, C. G. Faulkes, M. Selbach, G. R. Lewin, Hypofunctional TrkA accounts for the absence of pain sensitization in the African naked mole-rat. *Cell Reports* **17**, 748–758 (2016). [doi:10.1016/j.celrep.2016.09.035](https://doi.org/10.1016/j.celrep.2016.09.035) [Medline](#)
29. Z. Liu, W. Wang, T.-Z. Zhang, G.-H. Li, K. He, J.-F. Huang, X.-L. Jiang, R. W. Murphy, P. Shi, Repeated functional convergent effects of Nav1.7 on acid insensitivity in hibernating mammals. *Proc. Biol. Sci.* **281**, 20132950 (2013). [doi:10.1098/rspb.2013.2950](https://doi.org/10.1098/rspb.2013.2950) [Medline](#)
30. X. Pan, Z. Li, Q. Zhou, H. Shen, K. Wu, X. Huang, J. Chen, J. Zhang, X. Zhu, J. Lei, W. Xiong, H. Gong, B. Xiao, N. Yan, Structure of the human voltage-gated sodium channel Nav1.4 in complex with $\beta 1$. *Science* **362**, eaau2486 (2018). [doi:10.1126/science.aau2486](https://doi.org/10.1126/science.aau2486) [Medline](#)
31. N. Pedemonte, L. J. V. Galletta, Structure and function of TMEM16 proteins (anoctamins). *Physiol. Rev.* **94**, 419–459 (2014). [doi:10.1152/physrev.00039.2011](https://doi.org/10.1152/physrev.00039.2011) [Medline](#)
32. F. Huang, X. Wang, E. M. Ostertag, T. Nuwal, B. Huang, Y.-N. Jan, A. I. Basbaum, L. Y. Jan, TMEM16C facilitates Na⁺-activated K⁺ currents in rat sensory neurons and regulates pain processing. *Nat. Neurosci.* **16**, 1284–1290 (2013). [doi:10.1038/nn.3468](https://doi.org/10.1038/nn.3468) [Medline](#)
33. P. Wanitchakool, J. Ousingsawat, L. Sirianant, I. Cabrita, D. Faria, R. Schreiber, K. Kunzelmann, Cellular defects by deletion of ANO10 are due to deregulated local calcium signaling. *Cell. Signal.* **30**, 41–49 (2017). [doi:10.1016/j.cellsig.2016.11.006](https://doi.org/10.1016/j.cellsig.2016.11.006) [Medline](#)
34. K. Kang, S. R. Pulver, V. C. Panzano, E. C. Chang, L. C. Griffith, D. L. Theobald, P. A. Garrity, Analysis of *Drosophila* TRPA1 reveals an ancient origin for human chemical nociception. *Nature* **464**, 597–600 (2010). [doi:10.1038/nature08848](https://doi.org/10.1038/nature08848) [Medline](#)
35. O. M. Arenas, E. E. Zaharieva, A. Para, C. Vásquez-Doorman, C. P. Petersen, M. Gallio, Activation of planarian TRPA1 by reactive oxygen species reveals a conserved mechanism for animal nociception. *Nat. Neurosci.* **20**, 1686–1693 (2017). [doi:10.1038/s41593-017-0005-0](https://doi.org/10.1038/s41593-017-0005-0) [Medline](#)

36. M. Oda, M. Kurogi, Y. Kubo, O. Saitoh, Sensitivities of two zebrafish TRPA1 paralogs to chemical and thermal stimuli analyzed in heterologous expression systems. *Chem. Senses* **41**, 261–272 (2016). [doi:10.1093/chemse/bjv091](https://doi.org/10.1093/chemse/bjv091) [Medline](#)
37. S. Saito, N. Banzawa, N. Fukuta, C. T. Saito, K. Takahashi, T. Imagawa, T. Ohta, M. Tominaga, Heat and noxious chemical sensor, chicken TRPA1, as a target of bird repellents and identification of its structural determinants by multispecies functional comparison. *Mol. Biol. Evol.* **31**, 708–722 (2014). [doi:10.1093/molbev/msu001](https://doi.org/10.1093/molbev/msu001) [Medline](#)
38. C. E. Paulsen, J. P. Armache, Y. Gao, Y. Cheng, D. Julius, Structure of the TRPA1 ion channel suggests regulatory mechanisms. *Nature* **520**, 511–517 (2015). [doi:10.1038/nature14367](https://doi.org/10.1038/nature14367) [Medline](#)
39. L. A. Swayne, A. Mezghrani, A. Varrault, J. Chemin, G. Bertrand, S. Dalle, E. Bourinet, P. Lory, R. J. Miller, J. Nargeot, A. Monteil, The NALCN ion channel is activated by M3 muscarinic receptors in a pancreatic beta-cell line. *EMBO Rep.* **10**, 873–880 (2009). [doi:10.1038/embor.2009.125](https://doi.org/10.1038/embor.2009.125) [Medline](#)
40. M. Cochet-Bissuel, P. Lory, A. Monteil, The sodium leak channel, NALCN, in health and disease. *Front. Cell. Neurosci.* **8**, 132 (2014). [doi:10.3389/fncel.2014.00132](https://doi.org/10.3389/fncel.2014.00132) [Medline](#)
41. J. A. Brock, E. M. McLachlan, C. Belmonte, Tetrodotoxin-resistant impulses in single nociceptor nerve terminals in guinea-pig cornea. *J. Physiol.* **512**, 211–217 (1998). [doi:10.1111/j.1469-7793.1998.211bf.x](https://doi.org/10.1111/j.1469-7793.1998.211bf.x) [Medline](#)
42. Y. Y. Wang, R. B. Chang, S. D. Allgood, W. L. Silver, E. R. Liman, A TRPA1-dependent mechanism for the pungent sensation of weak acids. *J. Gen. Physiol.* **137**, 493–505 (2011). [doi:10.1085/jgp.201110615](https://doi.org/10.1085/jgp.201110615) [Medline](#)
43. S. Leclercq, J. C. Braekman, D. Daloze, J. M. Pasteels, in *Progress in the Chemistry of Organic Natural Products*, W. Herz, H. Falk, G. W. Kirby, R. E. Moore, Eds. (Springer, 2000), pp. 115–229.
44. M. Z. Li, S. J. Elledge, in *Gene Synthesis*, vol. 852 of *Methods in Molecular Biology (Methods and Protocols)*, J. Peccoud, Ed. (Humana Press, 2012), pp. 51–59.
45. A. M. Bolger, M. Lohse, B. Usadel, Trimmomatic: A flexible trimmer for Illumina sequence data. *Bioinformatics* **30**, 2114–2120 (2014). [doi:10.1093/bioinformatics/btu170](https://doi.org/10.1093/bioinformatics/btu170) [Medline](#)
46. K. D. Pruitt, G. R. Brown, S. M. Hiatt, F. Thibaud-Nissen, A. Astashyn, O. Ermolaeva, C. M. Farrell, J. Hart, M. J. Landrum, K. M. McGarvey, M. R. Murphy, N. A. O’Leary, S. Pujar, B. Rajput, S. H. Rangwala, L. D. Riddick, A. Shkeda, H. Sun, P. Tamez, R. E. Tully, C. Wallin, D. Webb, J. Weber, W. Wu, M. DiCuccio, P. Kitts, D. R. Maglott, T. D. Murphy, J. M. Ostell, RefSeq: An update on mammalian reference sequences. *Nucleic Acids Res.* **42** (D1), D756–D763 (2014). [doi:10.1093/nar/gkt1114](https://doi.org/10.1093/nar/gkt1114) [Medline](#)
47. X. Huang, A. Madan, CAP3: A DNA sequence assembly program. *Genome Res.* **9**, 868–877 (1999). [doi:10.1101/gr.9.9.868](https://doi.org/10.1101/gr.9.9.868) [Medline](#)
48. S. J. Salter, M. J. Cox, E. M. Turek, S. T. Calus, W. O. Cookson, M. F. Moffatt, P. Turner, J. Parkhill, N. J. Loman, A. W. Walker, Reagent and laboratory contamination can critically impact sequence-based microbiome analyses. *BMC Biol.* **12**, 87 (2014). [doi:10.1186/s12915-014-0087-z](https://doi.org/10.1186/s12915-014-0087-z) [Medline](#)

49. S. T. O’Neil, S. J. Emrich, Assessing de novo transcriptome assembly metrics for consistency and utility. *BMC Genomics* **14**, 465 (2013). [doi:10.1186/1471-2164-14-465](https://doi.org/10.1186/1471-2164-14-465) [Medline](#)
50. R. Smith-Unna, C. Bournnell, R. Patro, J. M. Hibberd, S. Kelly, TransRate: Reference-free quality assessment of de novo transcriptome assemblies. *Genome Res.* **26**, 1134–1144 (2016). [doi:10.1101/gr.196469.115](https://doi.org/10.1101/gr.196469.115) [Medline](#)
51. F. A. Simão, R. M. Waterhouse, P. Ioannidis, E. V. Kriventseva, E. M. Zdobnov, BUSCO: Assessing genome assembly and annotation completeness with single-copy orthologs. *Bioinformatics* **31**, 3210–3212 (2015). [doi:10.1093/bioinformatics/btv351](https://doi.org/10.1093/bioinformatics/btv351) [Medline](#)
52. K. Katoh, D. M. Standley, MAFFT multiple sequence alignment software version 7: Improvements in performance and usability. *Mol. Biol. Evol.* **30**, 772–780 (2013). [doi:10.1093/molbev/mst010](https://doi.org/10.1093/molbev/mst010) [Medline](#)
53. I. Sela, H. Ashkenazy, K. Katoh, T. Pupko, GUIDANCE2: Accurate detection of unreliable alignment regions accounting for the uncertainty of multiple parameters. *Nucleic Acids Res.* **43** (W1), W7–W14 (2015). [doi:10.1093/nar/gkv318](https://doi.org/10.1093/nar/gkv318) [Medline](#)
54. A. Stamatakis, RAxML-VI-HPC: Maximum likelihood-based phylogenetic analyses with thousands of taxa and mixed models. *Bioinformatics* **22**, 2688–2690 (2006). [doi:10.1093/bioinformatics/btl446](https://doi.org/10.1093/bioinformatics/btl446) [Medline](#)
55. Z. Yang, PAML 4: Phylogenetic analysis by maximum likelihood. *Mol. Biol. Evol.* **24**, 1586–1591 (2007). [doi:10.1093/molbev/msm088](https://doi.org/10.1093/molbev/msm088) [Medline](#)
56. M. A. Suchard, A. Rambaut, Many-core algorithms for statistical phylogenetics. *Bioinformatics* **25**, 1370–1376 (2009). [doi:10.1093/bioinformatics/btp244](https://doi.org/10.1093/bioinformatics/btp244) [Medline](#)
57. A. Conesa, P. Madrigal, S. Tarazona, D. Gomez-Cabrero, A. Cervera, A. McPherson, M. W. Szczesniak, D. J. Gaffney, L. L. Elo, X. Zhang, A. Mortazavi, A survey of best practices for RNA-seq data analysis. *Genome Biol.* **17**, 13 (2016). [doi:10.1186/s13059-016-0881-8](https://doi.org/10.1186/s13059-016-0881-8) [Medline](#)
58. B. Langmead, S. L. Salzberg, Fast gapped-read alignment with Bowtie 2. *Nat. Methods* **9**, 357–359 (2012). [doi:10.1038/nmeth.1923](https://doi.org/10.1038/nmeth.1923) [Medline](#)
59. H. Li, B. Handsaker, A. Wysoker, T. Fennell, J. Ruan, N. Homer, G. Marth, G. Abecasis, R. Durbin; 1000 Genome Project Data Processing Subgroup, The Sequence Alignment/Map format and SAMtools. *Bioinformatics* **25**, 2078–2079 (2009). [doi:10.1093/bioinformatics/btp352](https://doi.org/10.1093/bioinformatics/btp352) [Medline](#)
60. A. Roberts, H. Feng, L. Pachter, Fragment assignment in the cloud with eXpress-D. *BMC Bioinformatics* **14**, 358 (2013). [doi:10.1186/1471-2105-14-358](https://doi.org/10.1186/1471-2105-14-358) [Medline](#)
61. M. D. Robinson, D. J. McCarthy, G. K. Smyth, edgeR: A Bioconductor package for differential expression analysis of digital gene expression data. *Bioinformatics* **26**, 139–140 (2010). [doi:10.1093/bioinformatics/btp616](https://doi.org/10.1093/bioinformatics/btp616) [Medline](#)
62. M. D. Robinson, A. Oshlack, A scaling normalization method for differential expression analysis of RNA-seq data. *Genome Biol.* **11**, R25 (2010). [doi:10.1186/gb-2010-11-3-r25](https://doi.org/10.1186/gb-2010-11-3-r25) [Medline](#)

63. L. van der Maaten, G. Hinton, Visualizing data using t-SNE. *J. Mach. Learn. Res.* **9**, 2579–2605 (2008).
64. S. Whitmee, C. D. L. Orme, Predicting dispersal distance in mammals: A trait-based approach. *J. Anim. Ecol.* **82**, 211–221 (2013). [doi:10.1111/j.1365-2656.2012.02030.x](https://doi.org/10.1111/j.1365-2656.2012.02030.x) [Medline](#)
65. B. J. Haas, A. Papanicolaou, M. Yassour, M. Grabherr, P. D. Blood, J. Bowden, M. B. Couger, D. Eccles, B. Li, M. Lieber, M. D. MacManes, M. Ott, J. Orvis, N. Pochet, F. Strozzi, N. Weeks, R. Westerman, T. William, C. N. Dewey, R. Henschel, R. D. LeDuc, N. Friedman, A. Regev, De novo transcript sequence reconstruction from RNA-seq using the Trinity platform for reference generation and analysis. *Nat. Protoc.* **8**, 1494–1512 (2013). [doi:10.1038/nprot.2013.084](https://doi.org/10.1038/nprot.2013.084) [Medline](#)
66. M. Suyama, D. Torrents, P. Bork, PAL2NAL: Robust conversion of protein sequence alignments into the corresponding codon alignments. *Nucleic Acids Res.* **34**, W609–W612 (2006). [doi:10.1093/nar/gkl315](https://doi.org/10.1093/nar/gkl315) [Medline](#)
67. J. P. Bielawski, Z. Yang, A maximum likelihood method for detecting functional divergence at individual codon sites, with application to gene family evolution. *J. Mol. Evol.* **59**, 121–132 (2004). [doi:10.1007/s00239-004-2597-8](https://doi.org/10.1007/s00239-004-2597-8) [Medline](#)
68. C. J. Weadick, B. S. W. Chang, An improved likelihood ratio test for detecting site-specific functional divergence among clades of protein-coding genes. *Mol. Biol. Evol.* **29**, 1297–1300 (2012). [doi:10.1093/molbev/msr311](https://doi.org/10.1093/molbev/msr311) [Medline](#)
69. A. M. Waterhouse, J. B. Procter, D. M. A. Martin, M. Clamp, G. J. Barton, Jalview Version 2—A multiple sequence alignment editor and analysis workbench. *Bioinformatics* **25**, 1189–1191 (2009). [doi:10.1093/bioinformatics/btp033](https://doi.org/10.1093/bioinformatics/btp033) [Medline](#)